# SUPPLEMENTARY INFORMATION

## Functional interaction between FOXO3a and ATM regulates DNA damage response

Wen-Bin Tsai, Young Min Chung, Yoko Takahashi, Zhaohui Xu, and Mickey C-T. Hu*

*Correspondence should be addressed to M.C.T.H.
(e-mail: michu@mdanderson.org)

**Supplementary Figures: Figure S1- Figure S6**
**Legends for Supplementary Figures**
**Supplementary Text**
**Supplementary Materials and Methods**
**Supplementary References**

Fig. S1

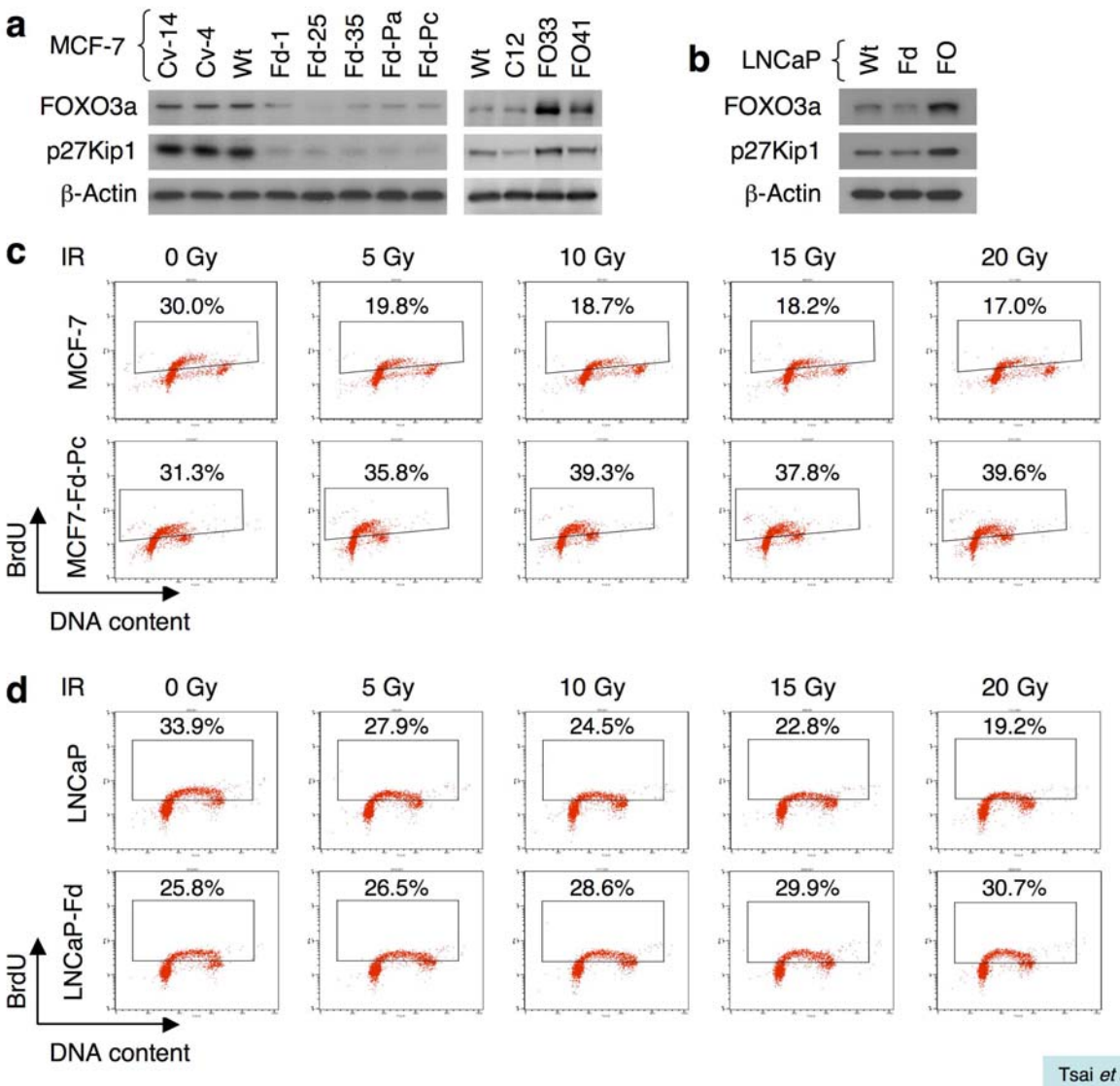


Tsai *et al.*, NCB-H11173C

Fig. S1

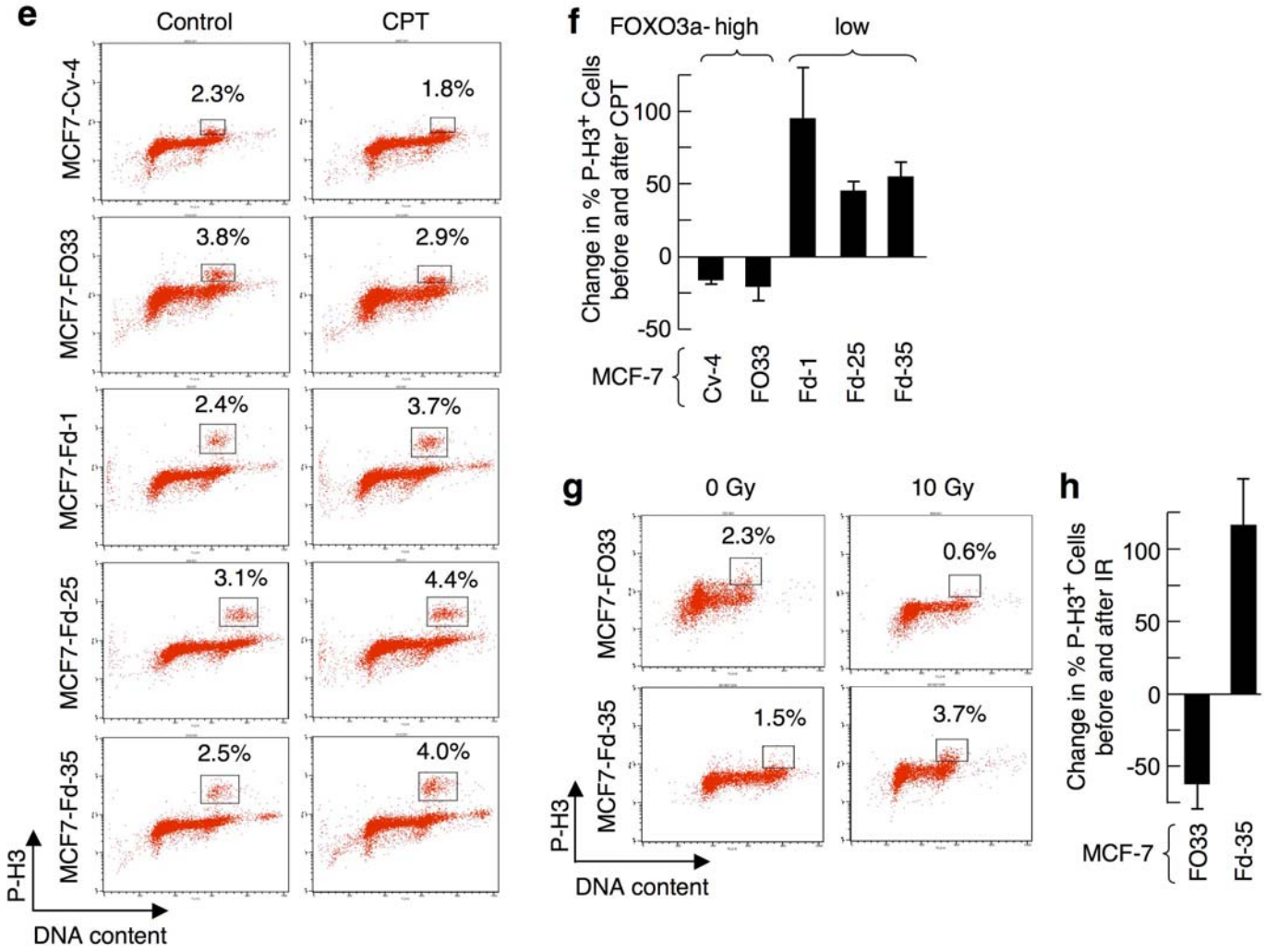


Tsai *et al.*, NCB-H11173C

Fig. S1

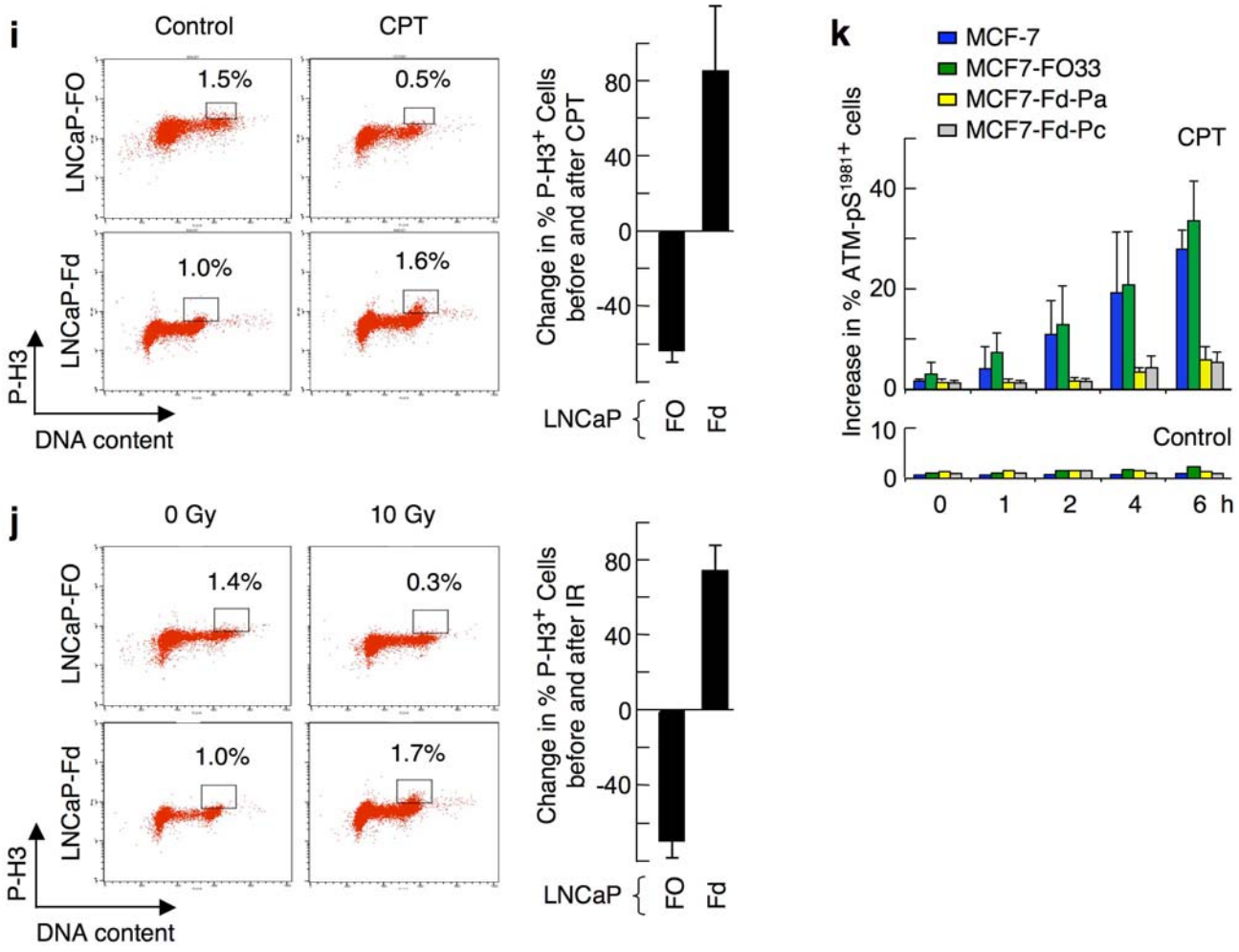


Tsai *et al.*, NCB-H11173C

Fig. S1

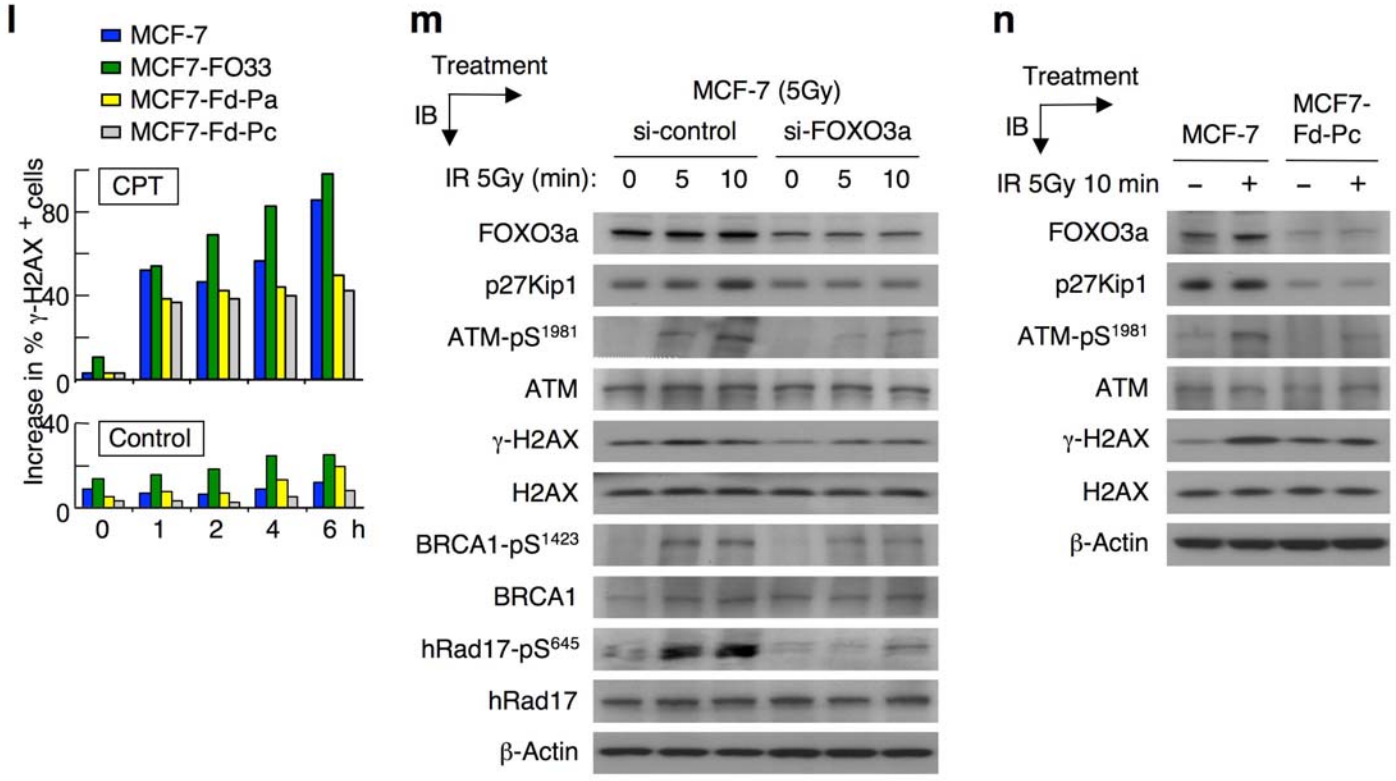
l
MCF-7
MCF7-FO33
MCF7-Fd-Pa
MCF7-Fd-Pc
CPT
Control
Increase in % γ-H2AX + cells
0
40
80
0 1 2 4 6 h
m
Treatment
IB
MCF-7 (5Gy)
si-control
si-FOXO3a
IR 5Gy (min): 0 5 10 0 5 10
FOXO3a
p27Kip1
ATM-pS1981
ATM
γ-H2AX
H2AX
BRCA1-pS1423
BRCA1
hRad17-pS645
hRad17
β-Actin
n
Treatment
IB
MCF-7
MCF7-Fd-Pc
IR 5Gy 10 min – + – +
FOXO3a
p27Kip1
ATM-pS1981
ATM
γ-H2AX
H2AX
β-Actin

Fig. S2

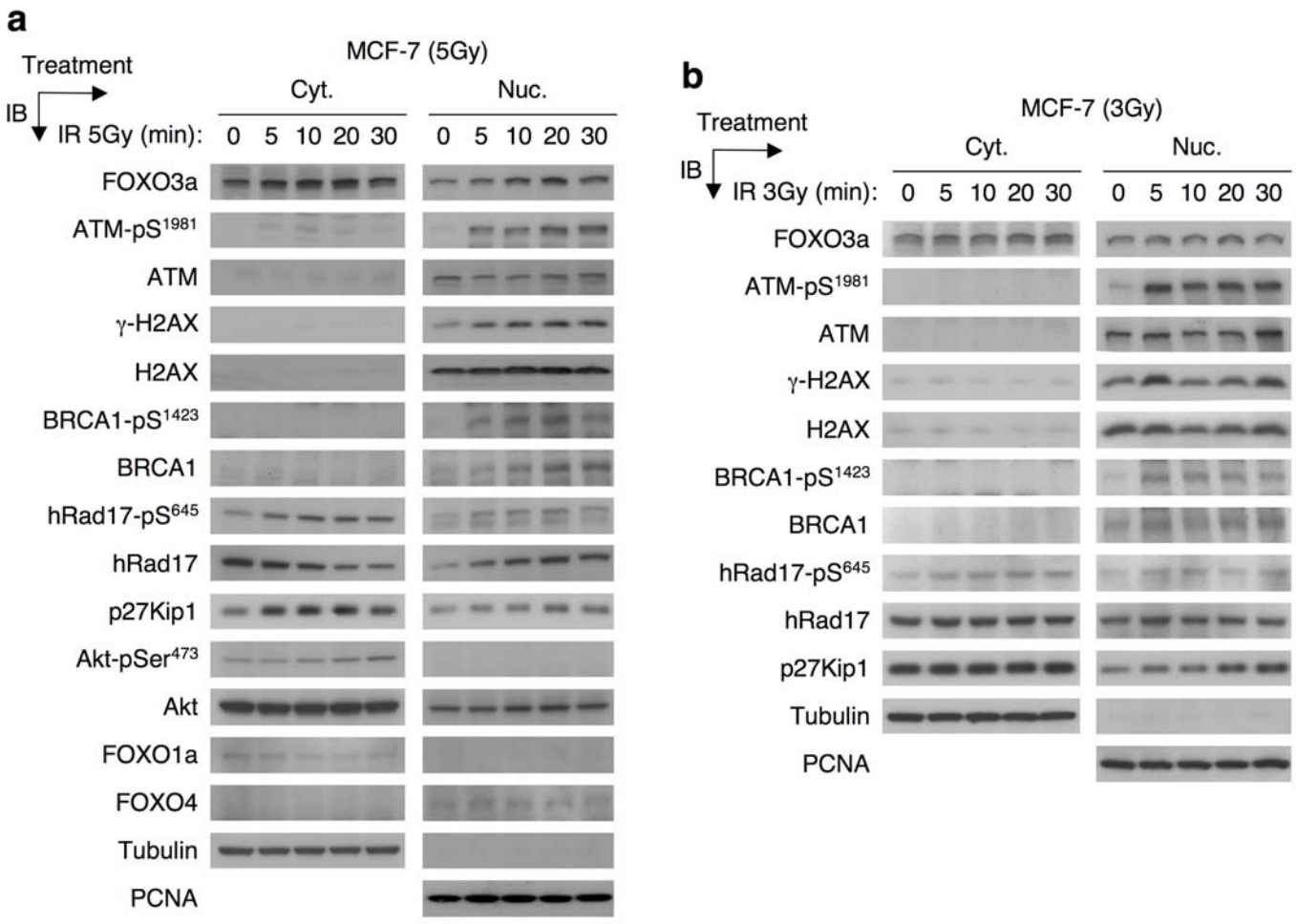
a
Treatment
IB
MCF-7 (5Gy)
Cyt.
Nuc.
IR 5Gy (min): 0 5 10 20 30 0 5 10 20 30
FOXO3a
ATM-pS1981
ATM
γ-H2AX
H2AX
BRCA1-pS1423
BRCA1
hRad17-pS645
hRad17
p27Kip1
Akt-pSer473
Akt
FOXO1a
FOXO4
Tubulin
PCNA
b
Treatment
IB
MCF-7 (3Gy)
Cyt.
Nuc.
IR 3Gy (min): 0 5 10 20 30 0 5 10 20 30
FOXO3a
ATM-pS1981
ATM
γ-H2AX
H2AX
BRCA1-pS1423
BRCA1
hRad17-pS645
hRad17
p27Kip1
Tubulin
PCNA

Fig. S2

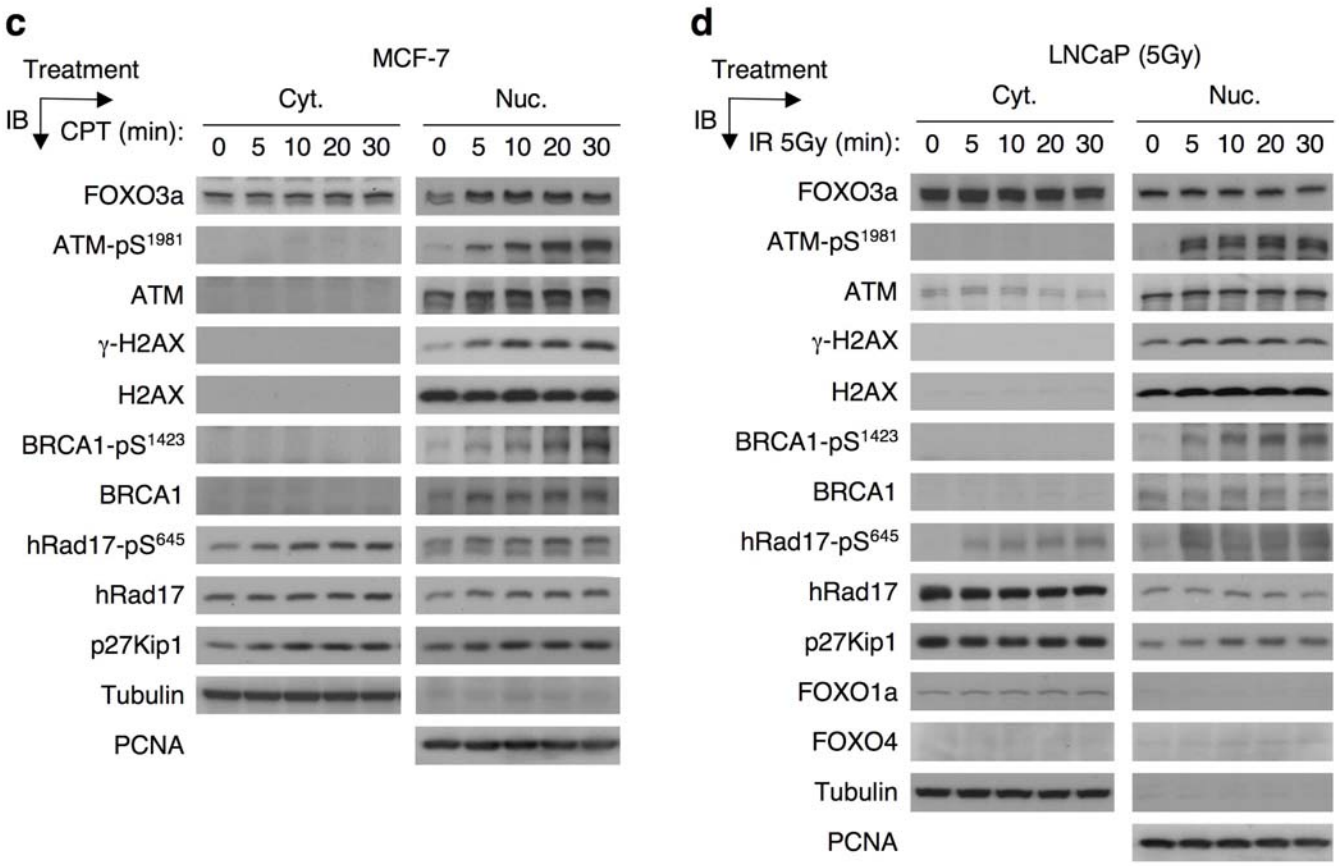
c
Treatment
IB
CPT (min):
MCF-7
Cyt.
Nuc.
0 5 10 20 30
0 5 10 20 30
FOXO3a
ATM-pS1981
ATM
γ-H2AX
H2AX
BRCA1-pS1423
BRCA1
hRad17-pS645
hRad17
p27Kip1
Tubulin
PCNA
d
Treatment
IB
IR 5Gy (min):
LNCaP (5Gy)
Cyt.
Nuc.
0 5 10 20 30
0 5 10 20 30
FOXO3a
ATM-pS1981
ATM
γ-H2AX
H2AX
BRCA1-pS1423
BRCA1
hRad17-pS645
hRad17
p27Kip1
FOXO1a
FOXO4
Tubulin
PCNA

Fig. S2

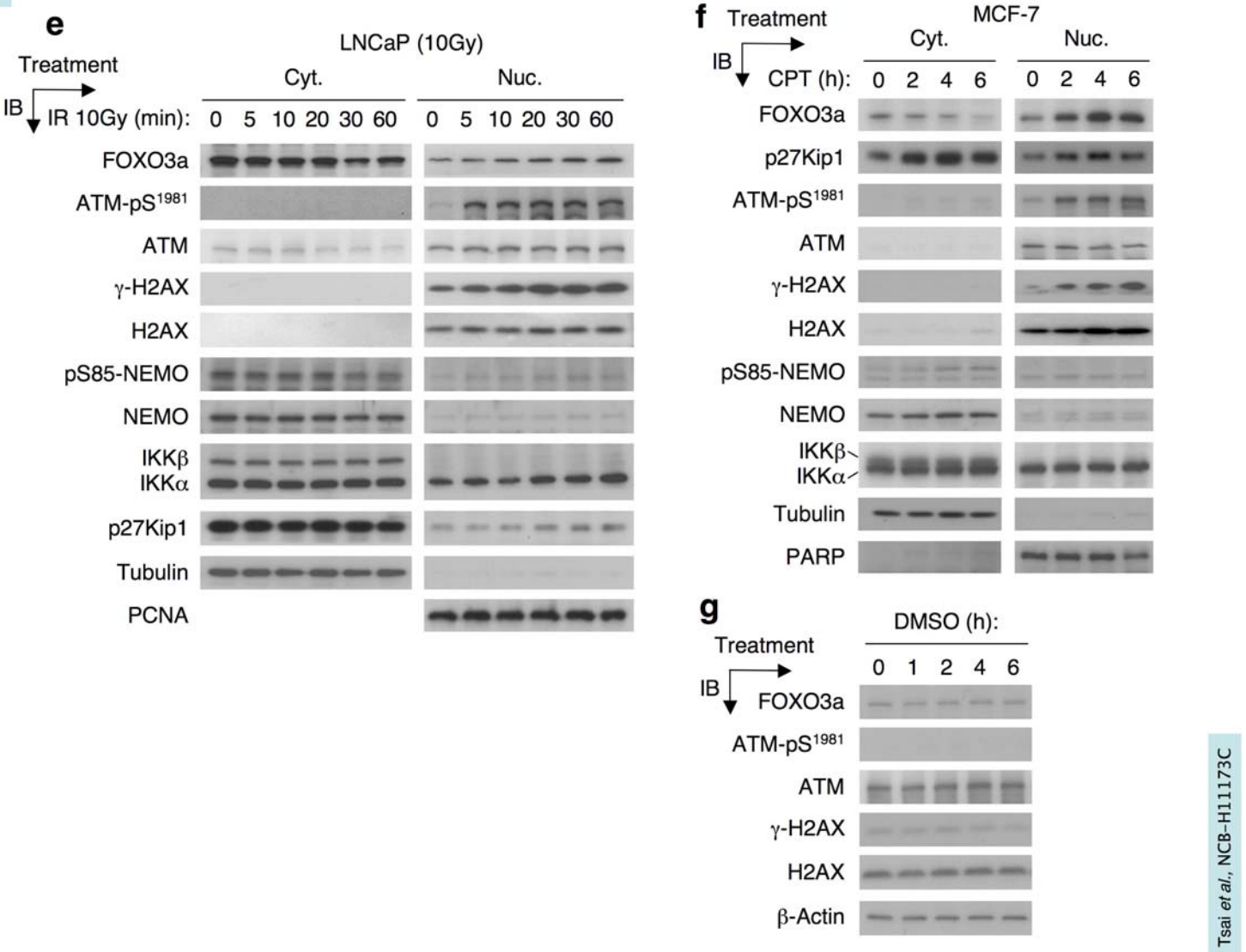

Fig. S3

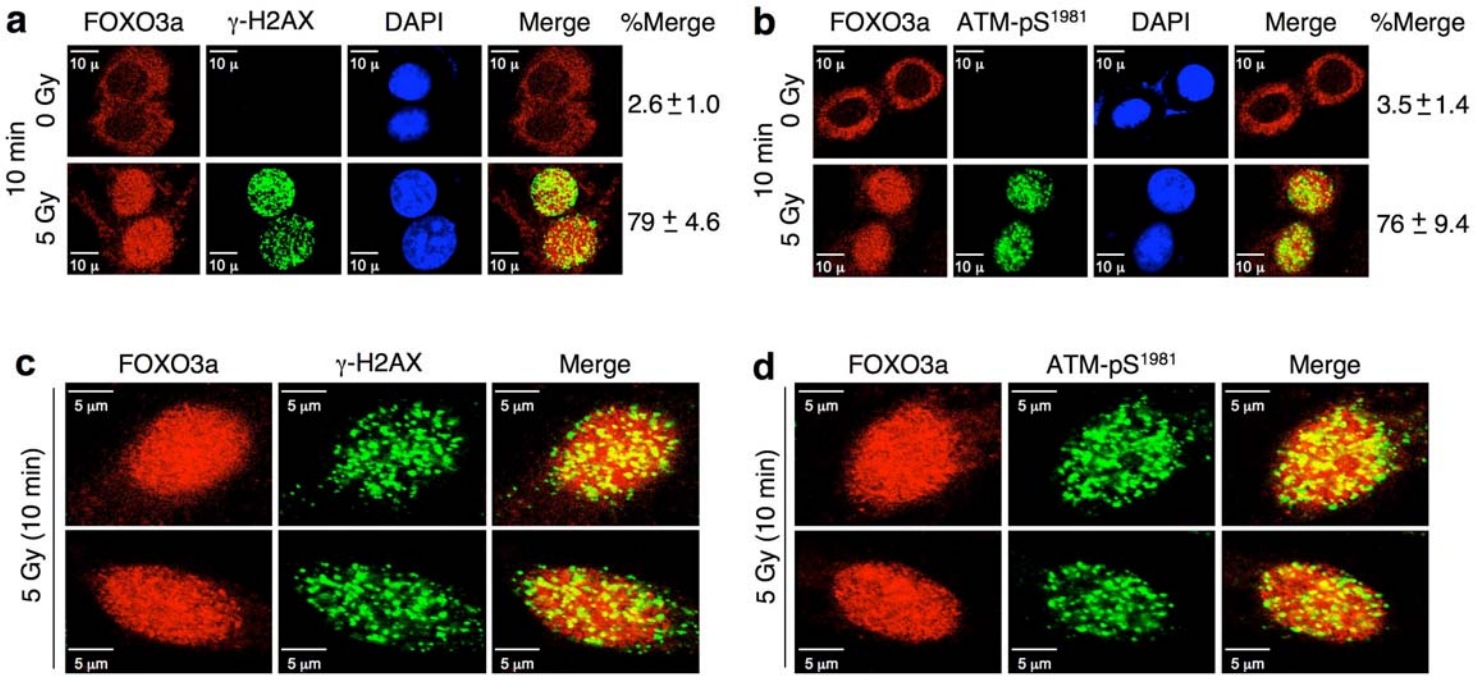
a
FOXO3a
γ-H2AX
DAPI
Merge
%Merge
10 min
0 Gy
5 Gy
2.6 ± 1.0
79 ± 4.6
b
FOXO3a
ATM-pS1981
DAPI
Merge
%Merge
3.5 ± 1.4
76 ± 9.4
c
FOXO3a
γ-H2AX
Merge
5 Gy (10 min)
d
FOXO3a
ATM-pS1981
Merge
5 Gy (10 min)

Fig. S3

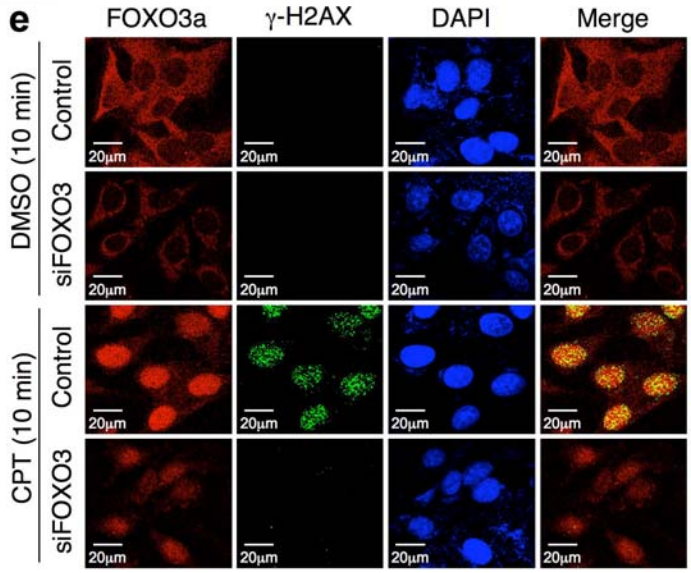


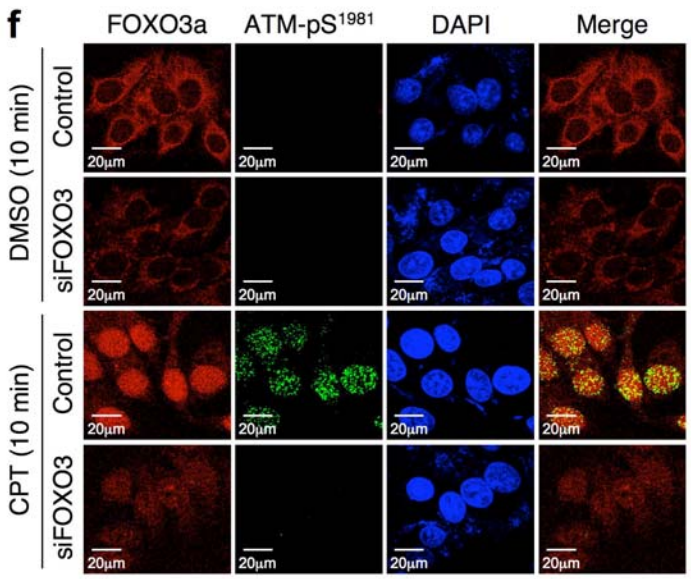


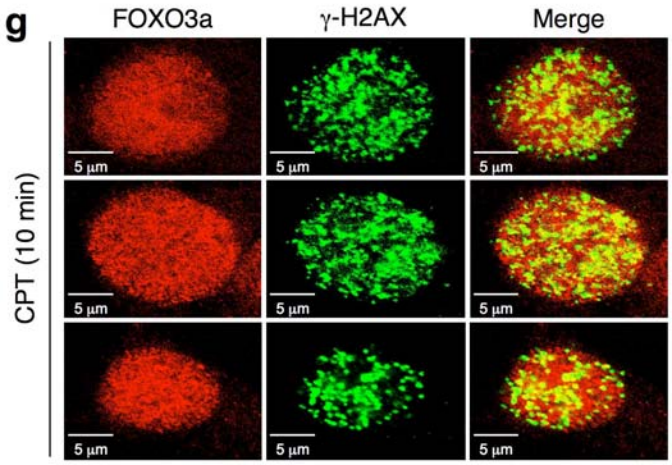


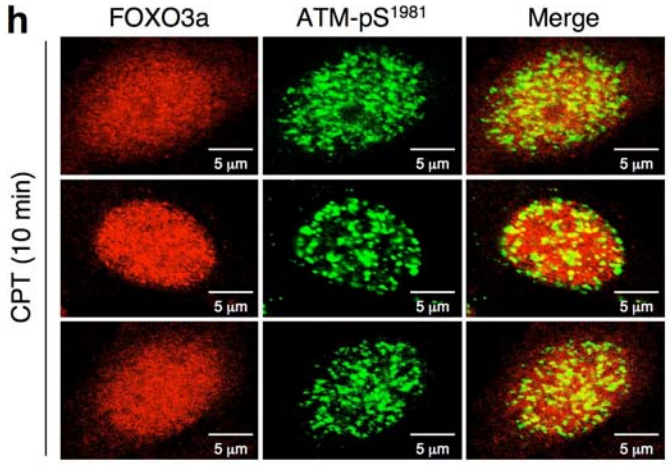


Tsai *et al.*, NCB-H11173C

Fig. S3

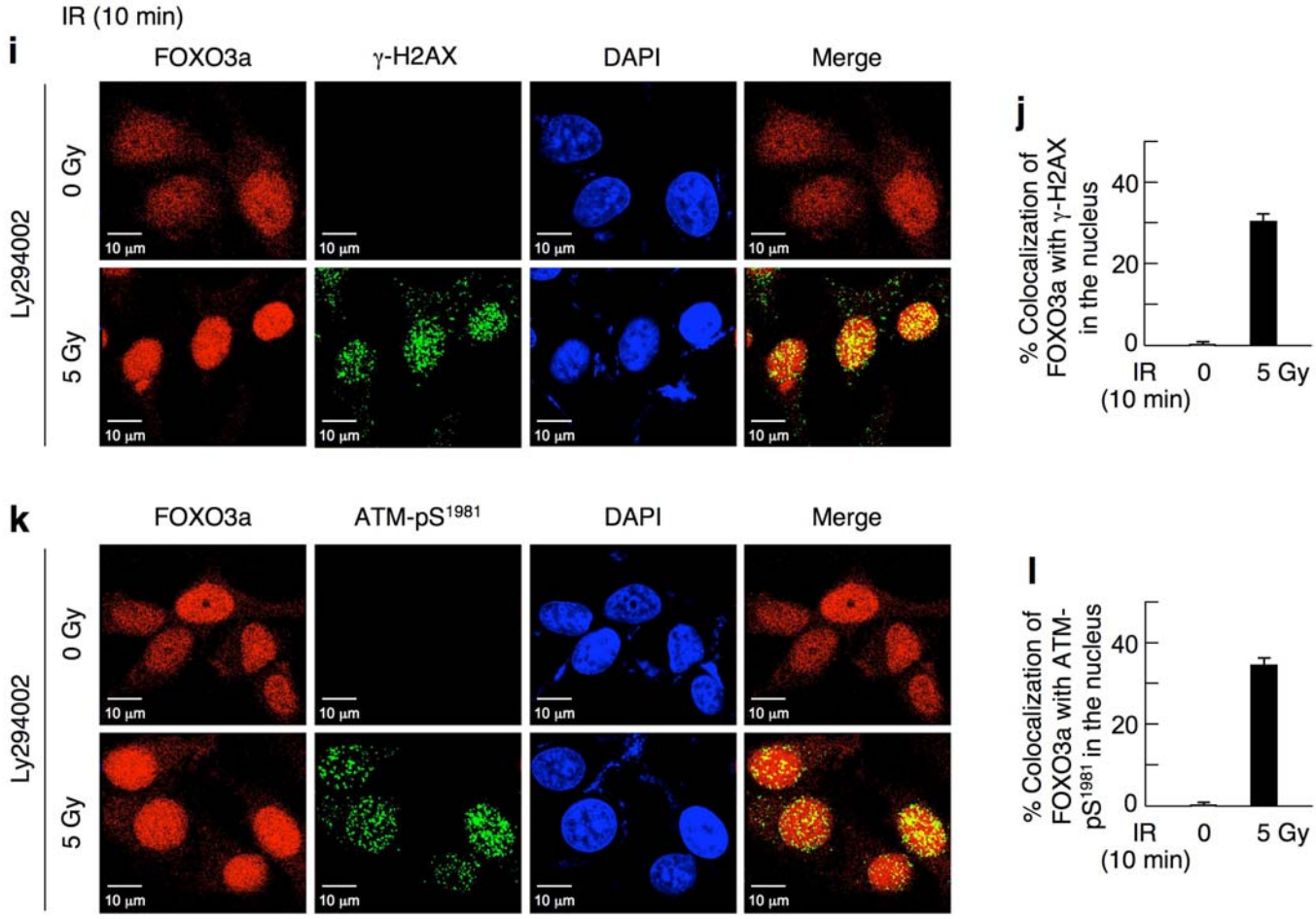
IR (10 min)
i
FOXO3a
γ-H2AX
DAPI
Merge
Ly294002
0 Gy
5 Gy
10 μm
j
% Colocalization of FOXO3a with γ-H2AX in the nucleus
40
20
0
IR
0
5 Gy
(10 min)
k
FOXO3a
ATM-pS1981
DAPI
Merge
Ly294002
0 Gy
5 Gy
10 μm
l
% Colocalization of FOXO3a with ATM-pS1981 in the nucleus
40
20
0
IR
0
5 Gy
(10 min)

Fig. S3

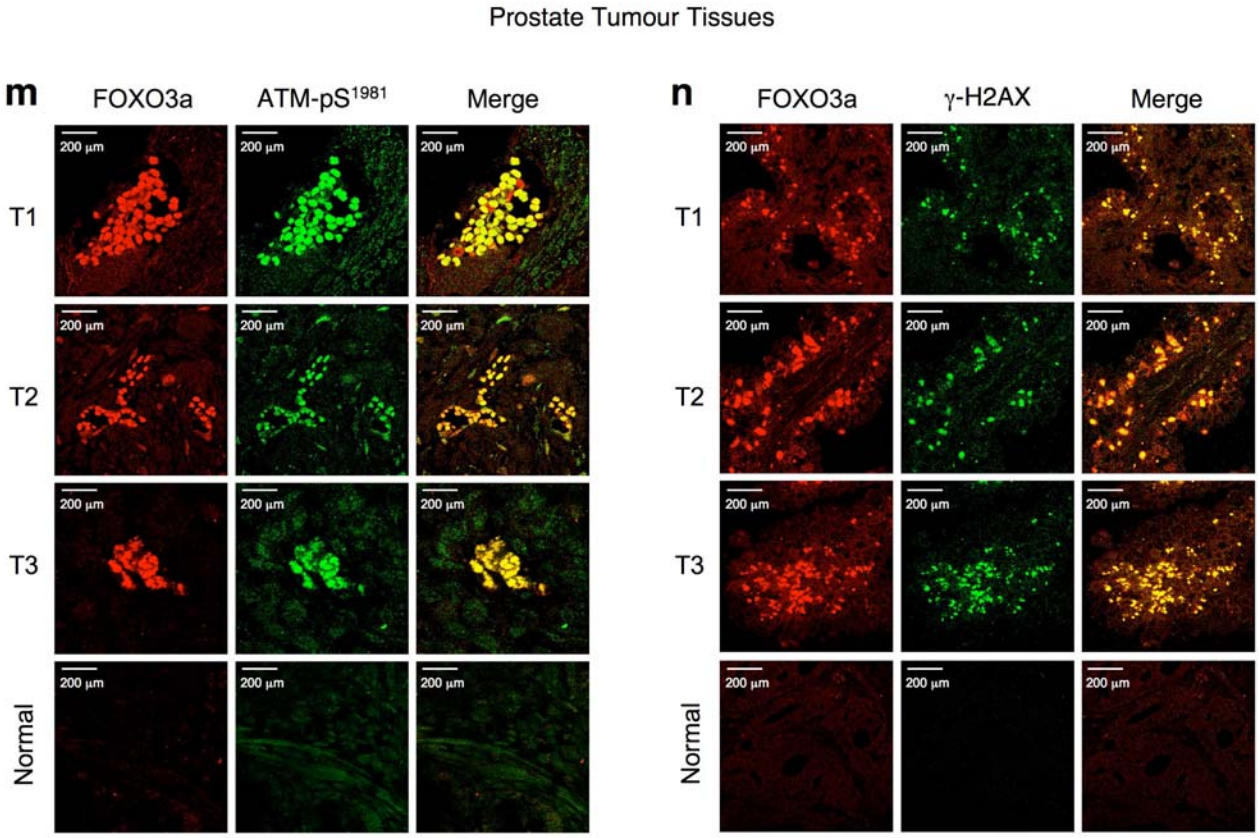


Tsai *et al.*, NCB-H11173C

Fig. S3

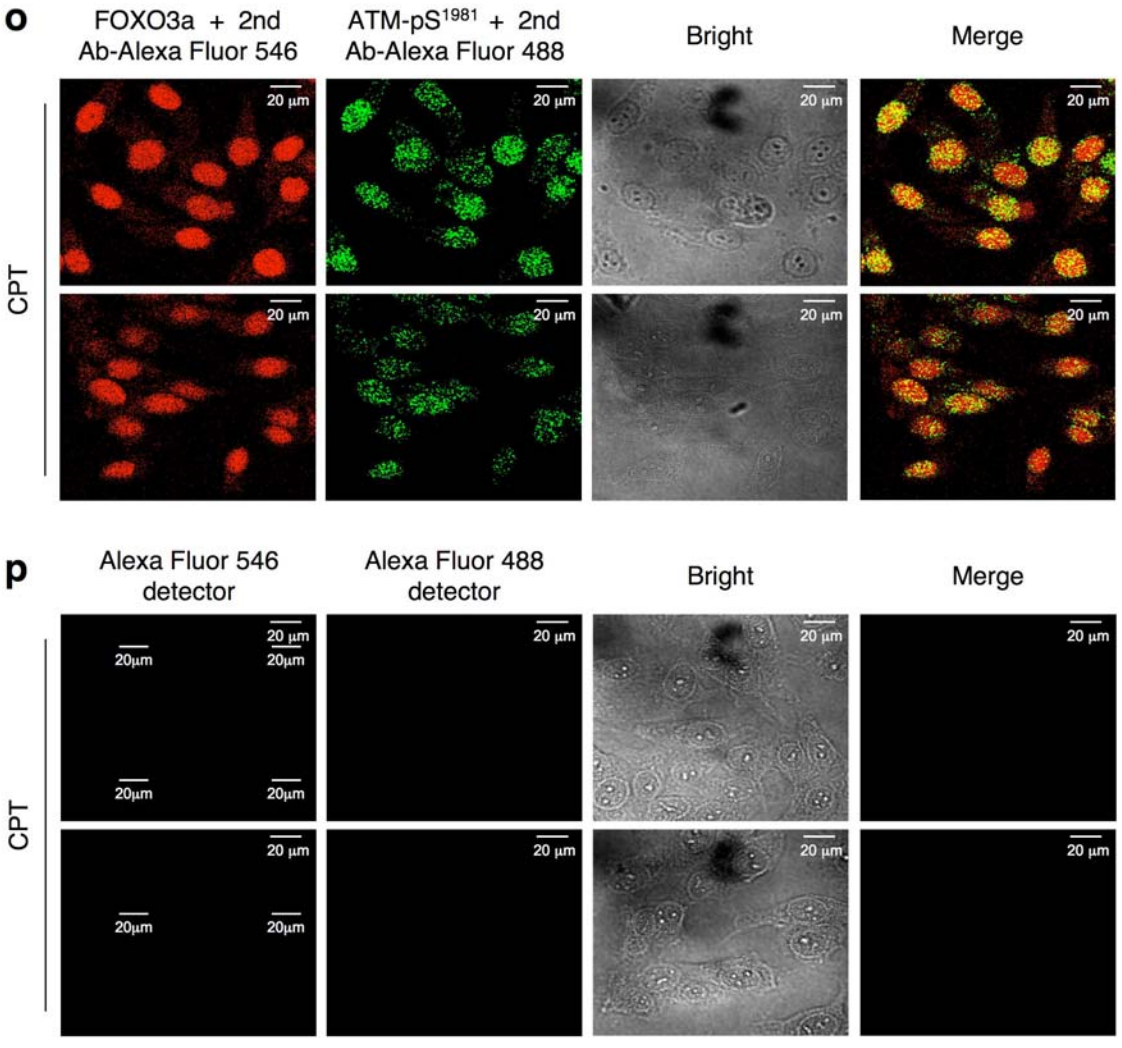
o
FOXO3a + 2nd Ab-Alexa Fluor 546
ATM-pS1981 + 2nd Ab-Alexa Fluor 488
Bright
Merge
CPT
20 μm
p
Alexa Fluor 546 detector
Alexa Fluor 488 detector
Bright
Merge
CPT
20μm

Fig. S4

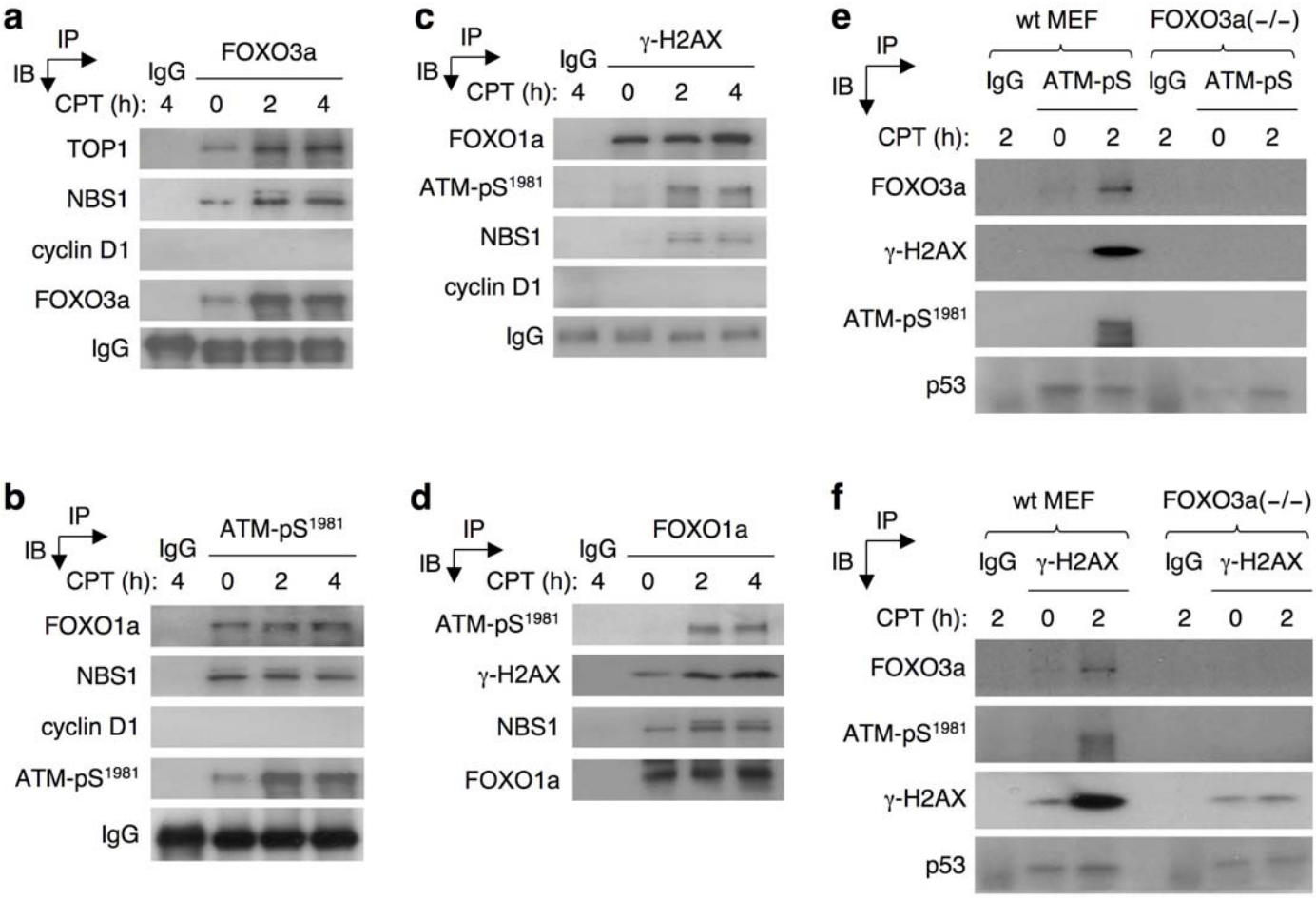
a
IP
IB
IgG
FOXO3a
CPT (h): 4 0 2 4
TOP1
NBS1
cyclin D1
FOXO3a
IgG
c
IP
IB
IgG
γ-H2AX
CPT (h): 4 0 2 4
FOXO1a
ATM-pS1981
NBS1
cyclin D1
IgG
e
wt MEF
FOXO3a(−/−)
IP
IB
IgG ATM-pS IgG ATM-pS
CPT (h): 2 0 2 2 0 2
FOXO3a
γ-H2AX
ATM-pS1981
p53
b
IP
IB
IgG
ATM-pS1981
CPT (h): 4 0 2 4
FOXO1a
NBS1
cyclin D1
ATM-pS1981
IgG
d
IP
IB
IgG
FOXO1a
CPT (h): 4 0 2 4
ATM-pS1981
γ-H2AX
NBS1
FOXO1a
f
wt MEF
FOXO3a(−/−)
IP
IB
IgG γ-H2AX IgG γ-H2AX
CPT (h): 2 0 2 2 0 2
FOXO3a
ATM-pS1981
γ-H2AX
p53

Fig. S4

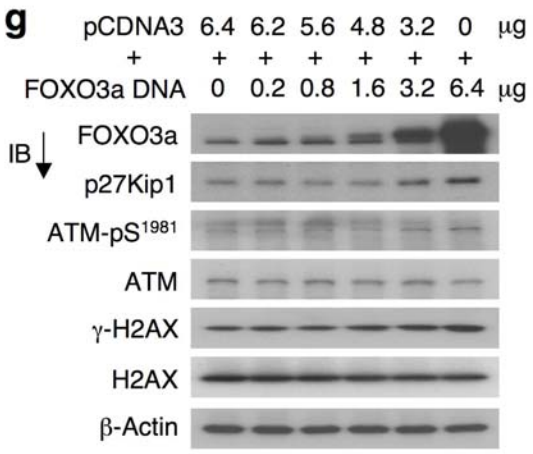
g
pCDNA3 6.4 6.2 5.6 4.8 3.2 0 μg
+ + + + + + +
FOXO3a DNA 0 0.2 0.8 1.6 3.2 6.4 μg
IB
FOXO3a
p27Kip1
ATM-pS1981
ATM
γ-H2AX
H2AX
β-Actin

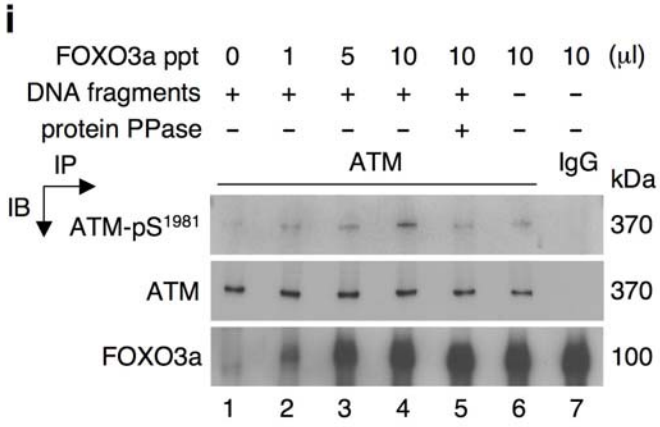
i
FOXO3a ppt 0 1 5 10 10 10 10 (μl)
DNA fragments + + + + + – –
protein PPase – – – – + – –
IP
ATM
IgG
kDa
IB
ATM-pS1981
370
ATM
370
FOXO3a
100
1 2 3 4 5 6 7

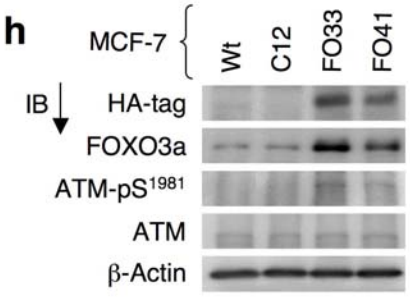
h
MCF-7
Wt
C12
FO33
FO41
IB
HA-tag
FOXO3a
ATM-pS1981
ATM
β-Actin

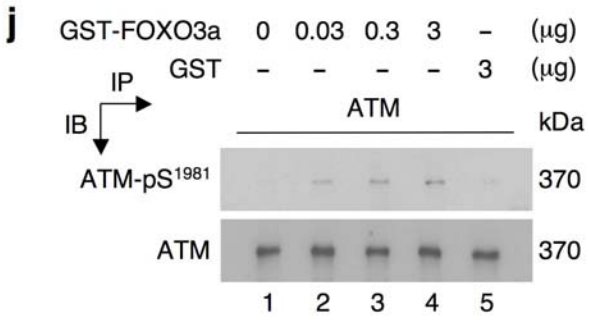
j
GST-FOXO3a 0 0.03 0.3 3 – (μg)
GST – – – – 3 (μg)
IP
ATM
kDa
IB
ATM-pS1981
370
ATM
370
1 2 3 4 5

Fig. S4

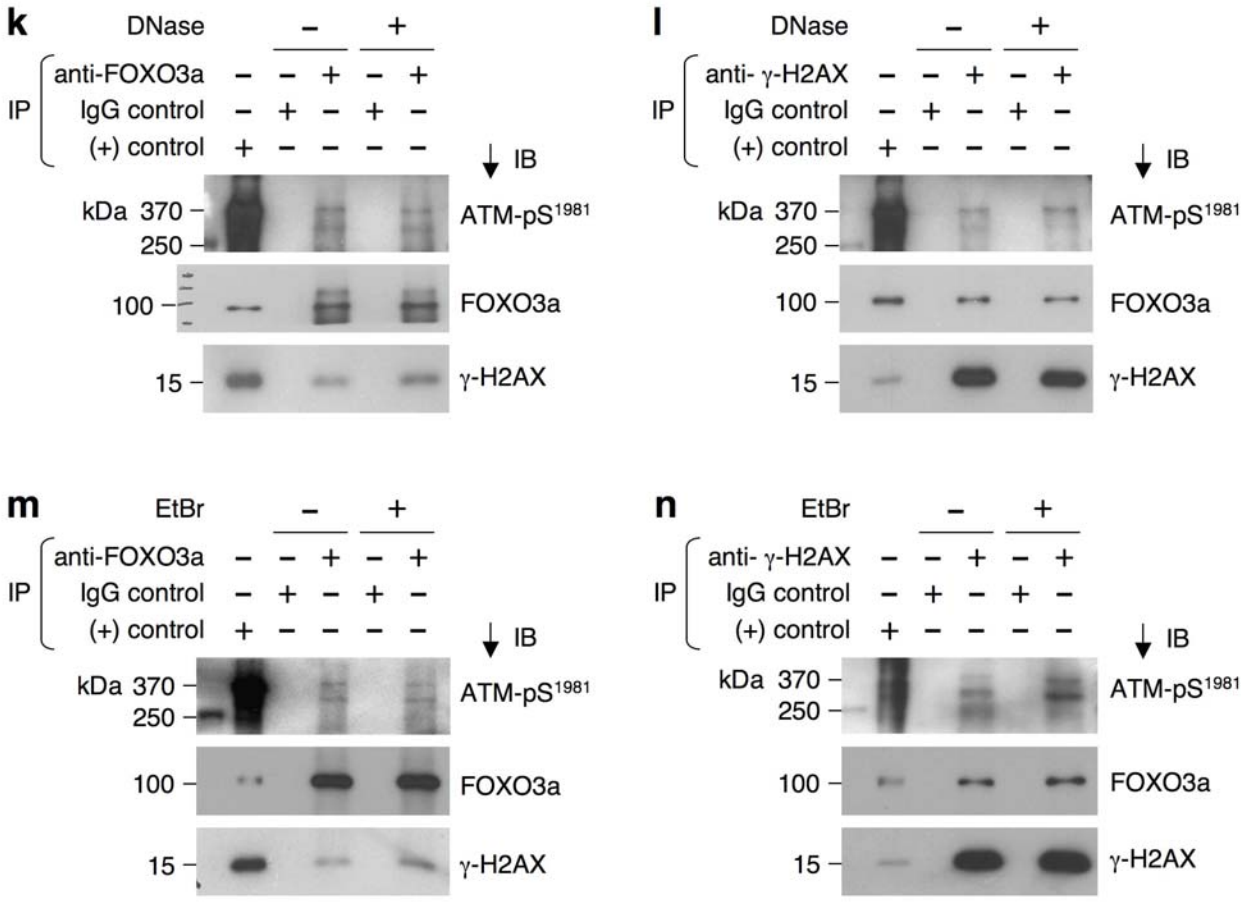
k
DNase
–
+
IP
anti-FOXO3a – – + – +
IgG control – + – + –
(+) control + – – – –
↓ IB
kDa 370
250
100
15
ATM-pS1981
FOXO3a
γ-H2AX
l
DNase
–
+
IP
anti- γ-H2AX – – + – +
IgG control – + – + –
(+) control + – – – –
↓ IB
kDa 370
250
100
15
ATM-pS1981
FOXO3a
γ-H2AX
m
EtBr
–
+
IP
anti-FOXO3a – – + – +
IgG control – + – + –
(+) control + – – – –
↓ IB
kDa 370
250
100
15
ATM-pS1981
FOXO3a
γ-H2AX
n
EtBr
–
+
IP
anti- γ-H2AX – – + – +
IgG control – + – + –
(+) control + – – – –
↓ IB
kDa 370
250
100
15
ATM-pS1981
FOXO3a
γ-H2AX

Fig. S4

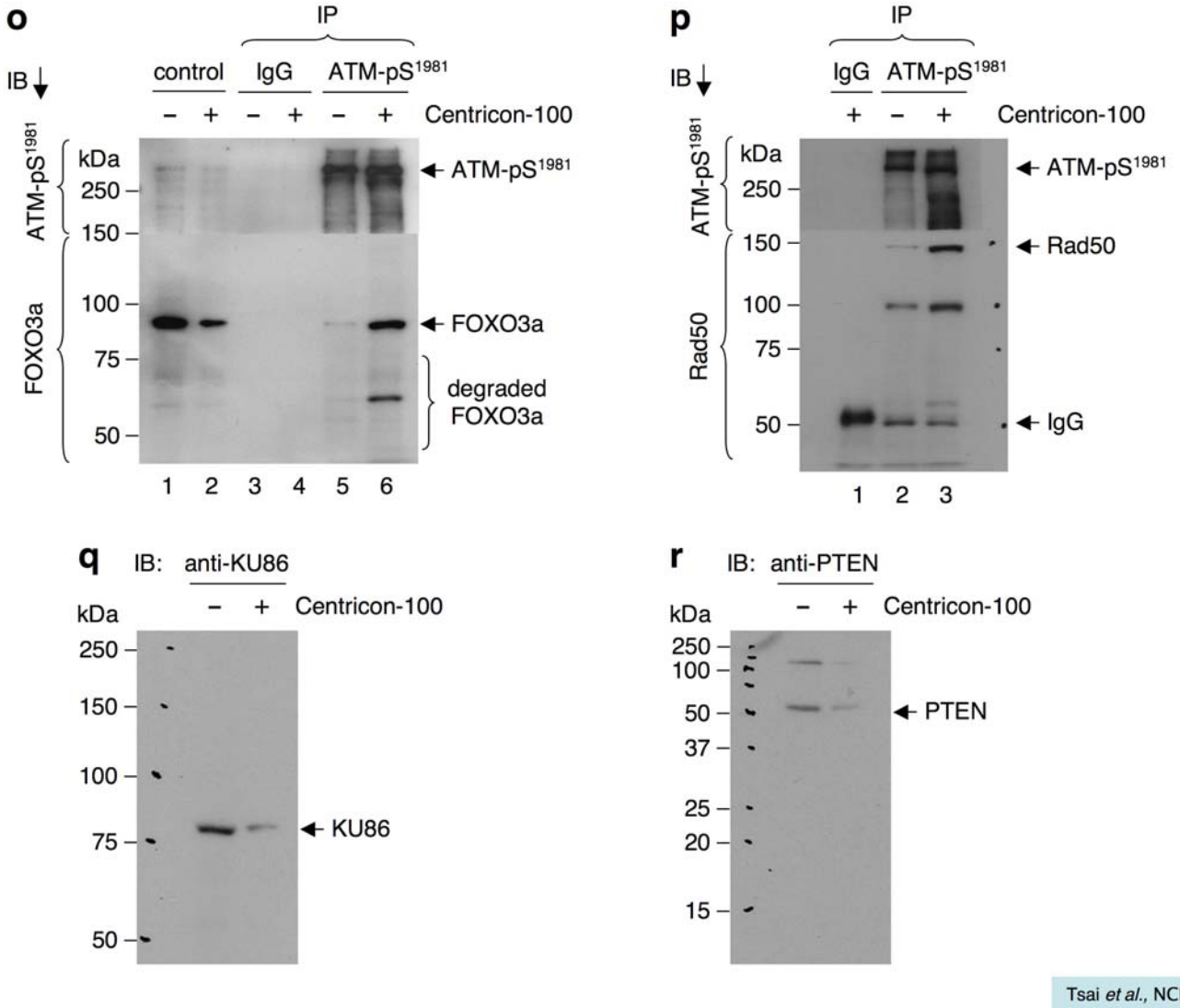


Tsai *et al.*, NCB-H11173C

Fig. S5

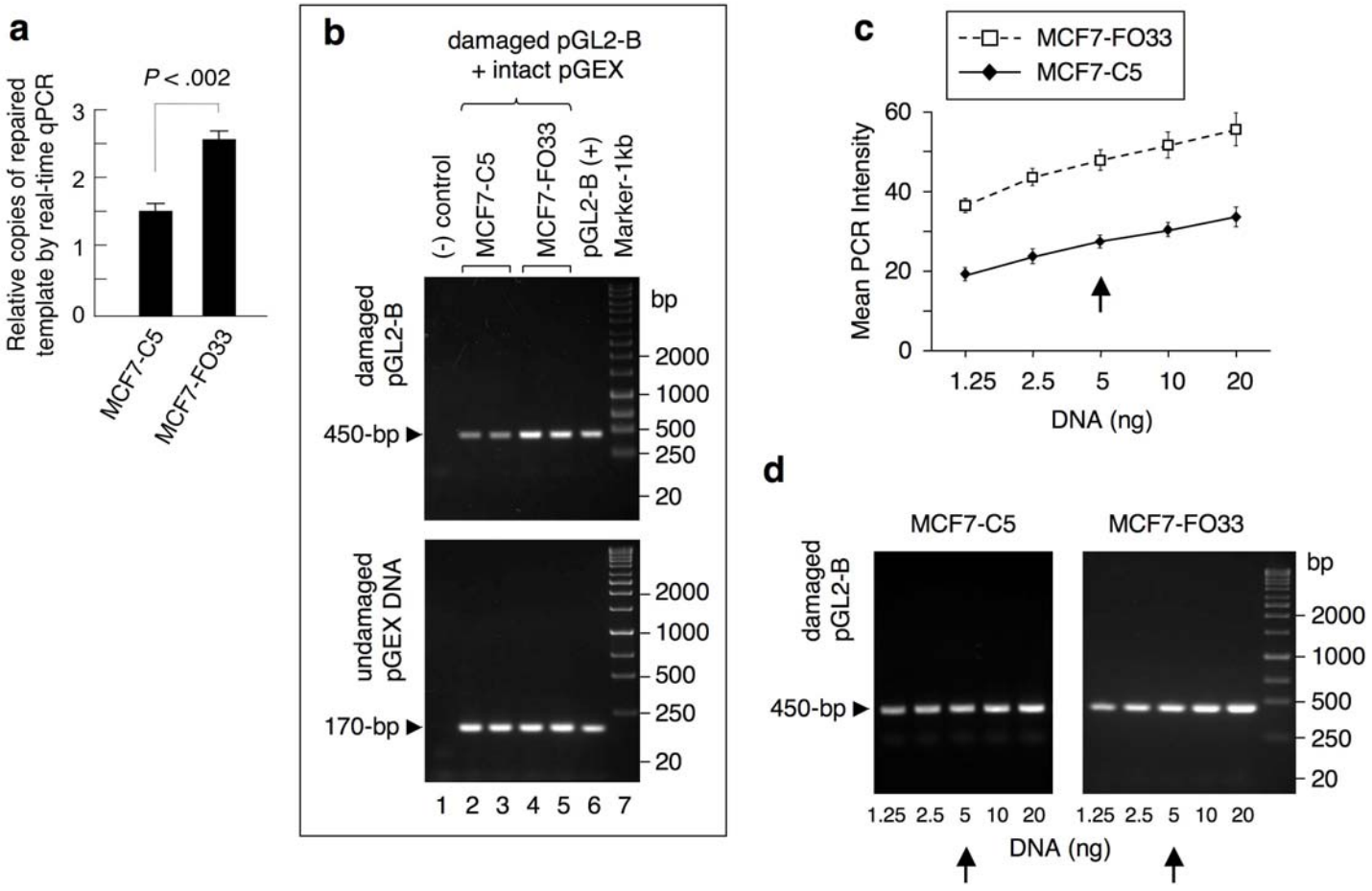
a
P < .002
Relative copies of repaired template by real-time qPCR
3
2
1
0
MCF7-C5
MCF7-FO33
b
damaged pGL2-B + intact pGEX
(-) control
MCF7-C5
MCF7-FO33
pGL2-B (+)
Marker-1kb
damaged pGL2-B
450-bp
undamaged pGEX DNA
170-bp
bp
2000
1000
500
250
20
1 2 3 4 5 6 7
c
MCF7-FO33
MCF7-C5
Mean PCR Intensity
60
40
20
0
1.25 2.5 5 10 20
DNA (ng)
d
MCF7-C5
MCF7-FO33
damaged pGL2-B
450-bp
bp
2000
1000
500
250
20
1.25 2.5 5 10 20
1.25 2.5 5 10 20
DNA (ng)

Fig. S5

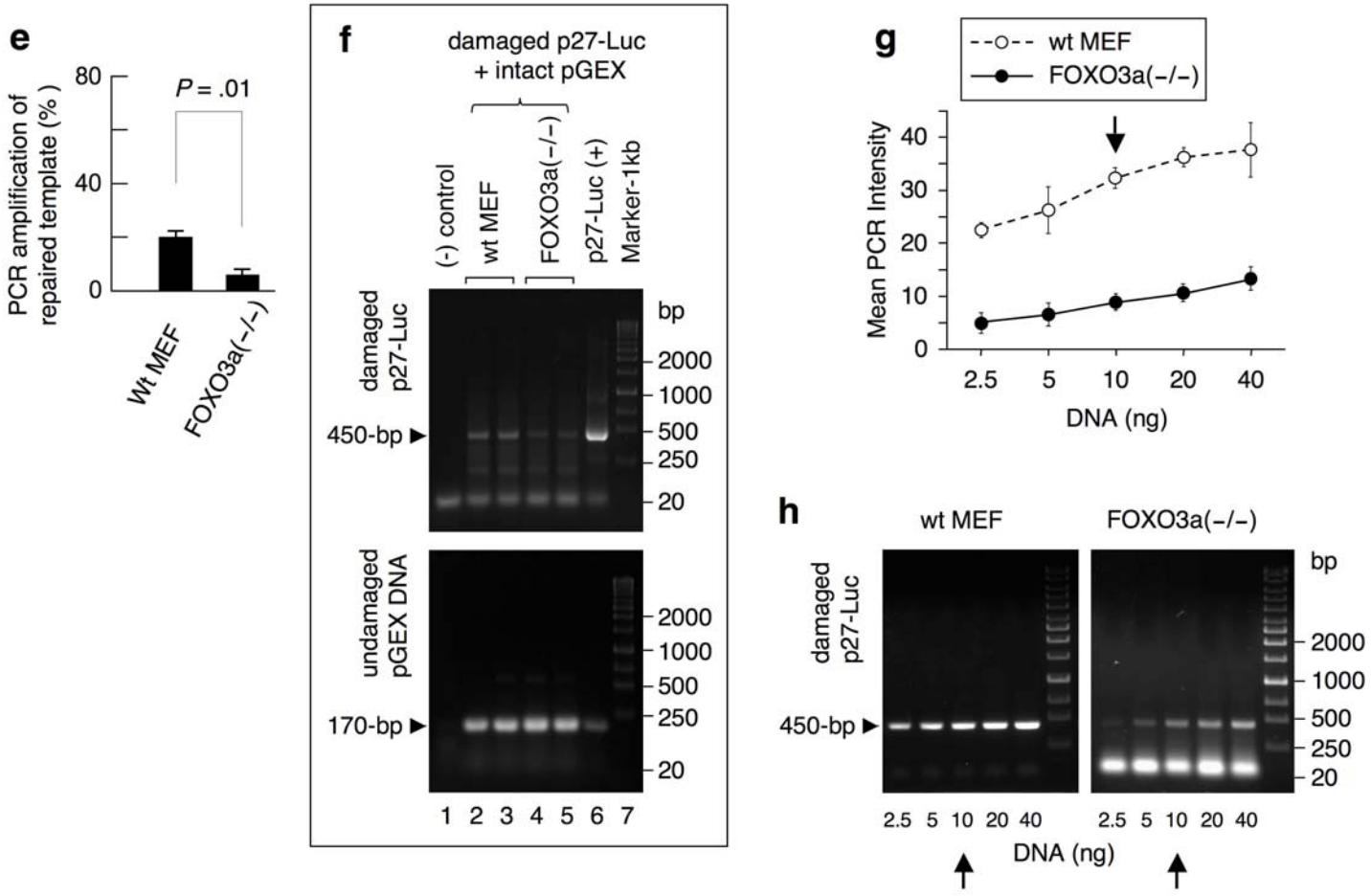
e
PCR amplification of repaired template (%)
80
40
0
P = .01
Wt MEF
FOXO3a(−/−)
f
damaged p27-Luc + intact pGEX
(-) control
wt MEF
FOXO3a(−/−)
p27-Luc (+)
Marker-1kb
damaged p27-Luc
450-bp
undamaged pGEX DNA
170-bp
bp
2000
1000
500
250
20
1 2 3 4 5 6 7
g
wt MEF
FOXO3a(−/−)
Mean PCR Intensity
40
30
20
10
0
2.5 5 10 20 40
DNA (ng)
h
wt MEF
FOXO3a(−/−)
damaged p27-Luc
450-bp
bp
2000
1000
500
250
20
2.5 5 10 20 40
2.5 5 10 20 40
DNA (ng)

Fig. S5

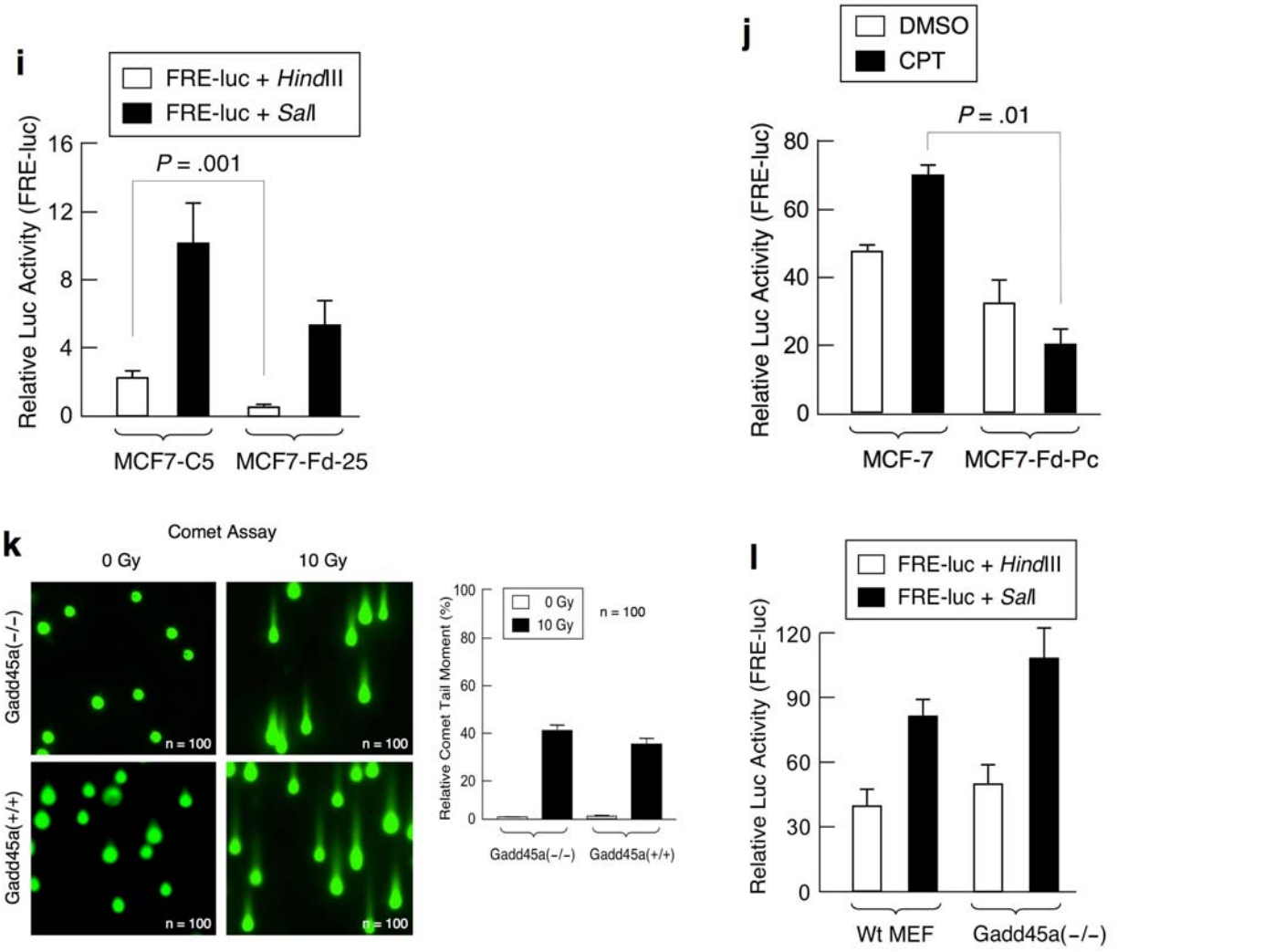


Tsai *et al.*, NCB-H11173C

Fig. S5

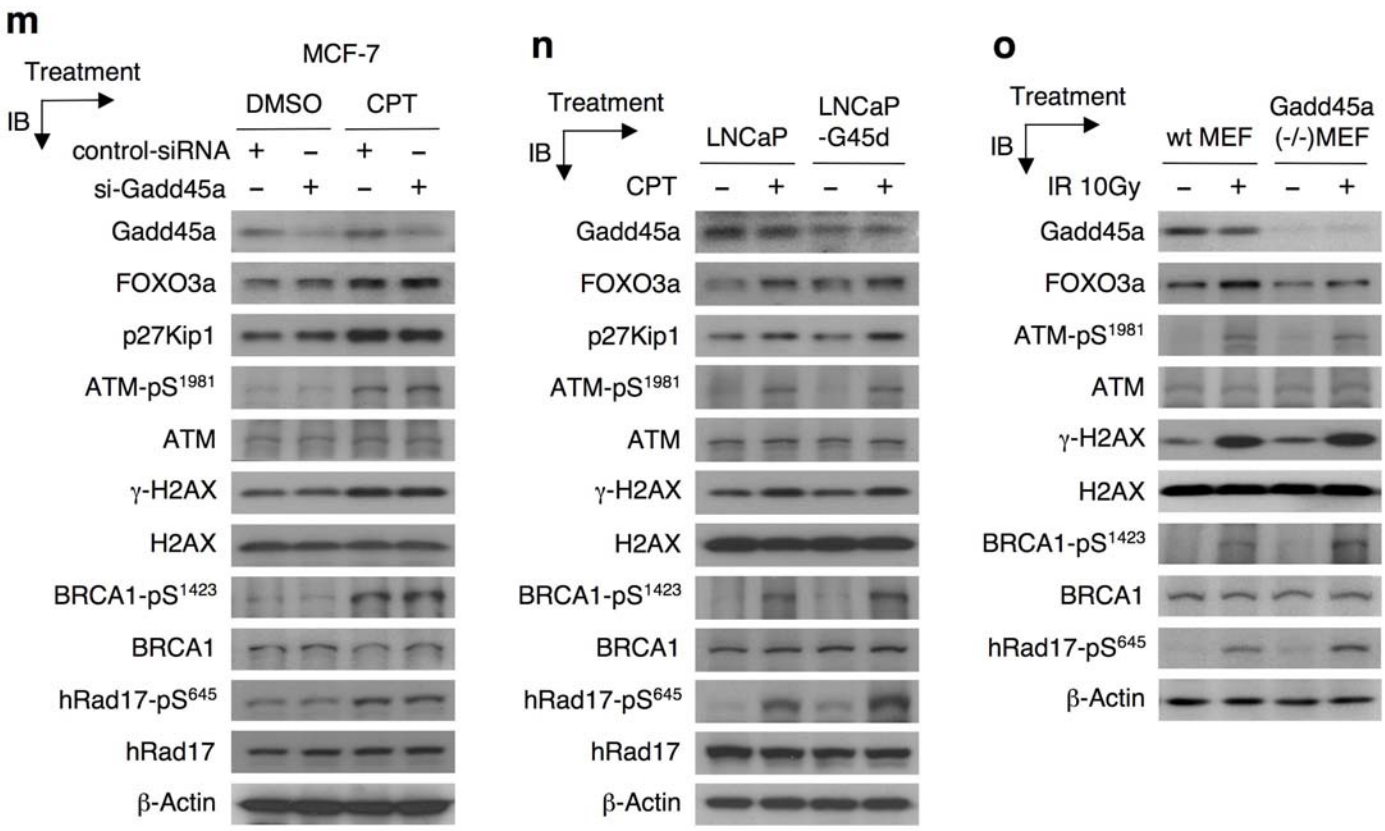
m
Treatment
IB
MCF-7
DMSO
CPT
control-siRNA + – + –
si-Gadd45a – + – +
Gadd45a
FOXO3a
p27Kip1
ATM-pS1981
ATM
γ-H2AX
H2AX
BRCA1-pS1423
BRCA1
hRad17-pS645
hRad17
β-Actin
n
Treatment
IB
LNCaP
LNCaP -G45d
CPT – + – +
Gadd45a
FOXO3a
p27Kip1
ATM-pS1981
ATM
γ-H2AX
H2AX
BRCA1-pS1423
BRCA1
hRad17-pS645
hRad17
β-Actin
o
Treatment
IB
wt MEF
Gadd45a (-/-)MEF
IR 10Gy – + – +
Gadd45a
FOXO3a
ATM-pS1981
ATM
γ-H2AX
H2AX
BRCA1-pS1423
BRCA1
hRad17-pS645
β-Actin

Fig. S6

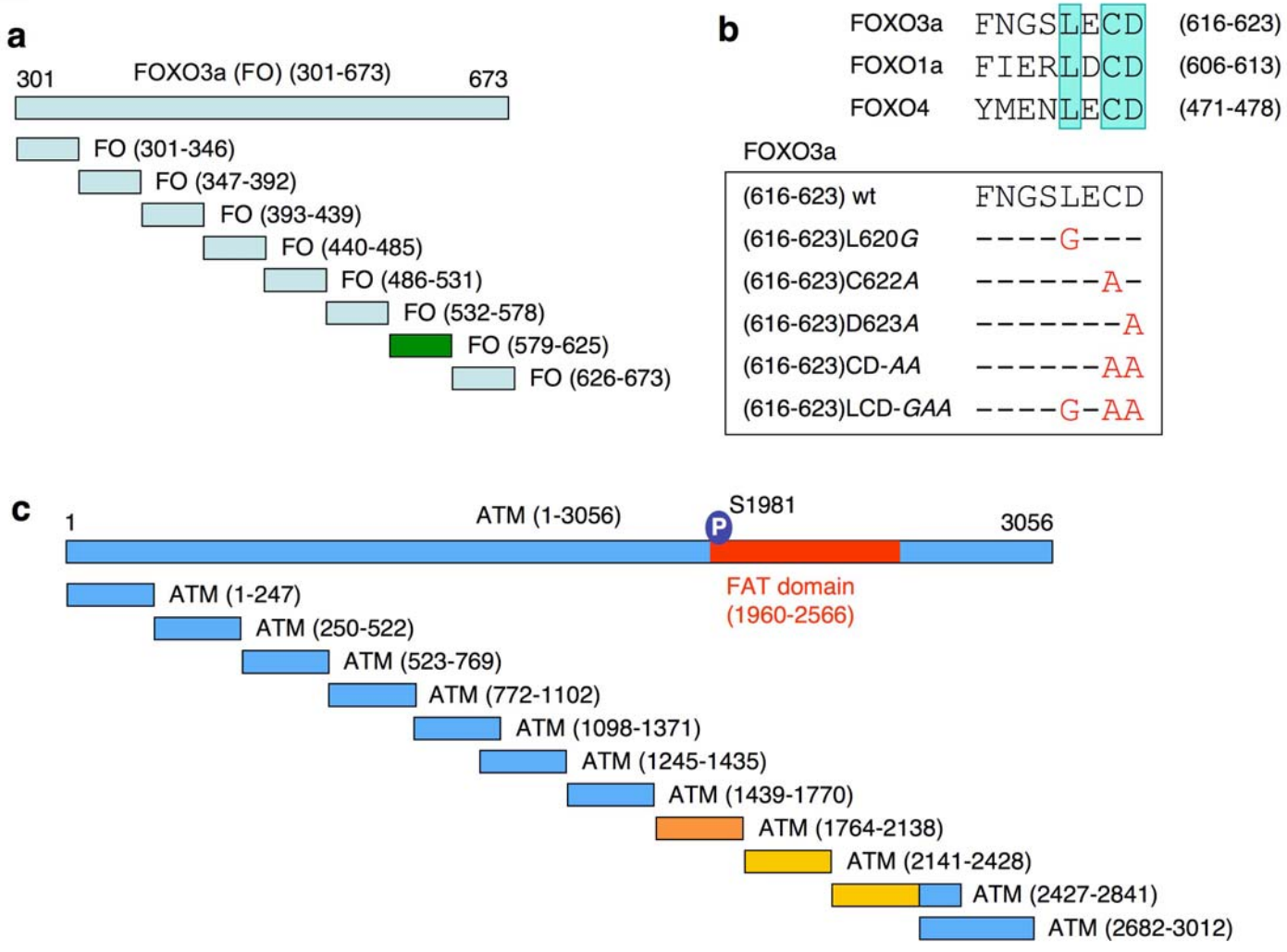


Tsai *et al.*, NCB-H11173C

Fig. S6 (full gels)

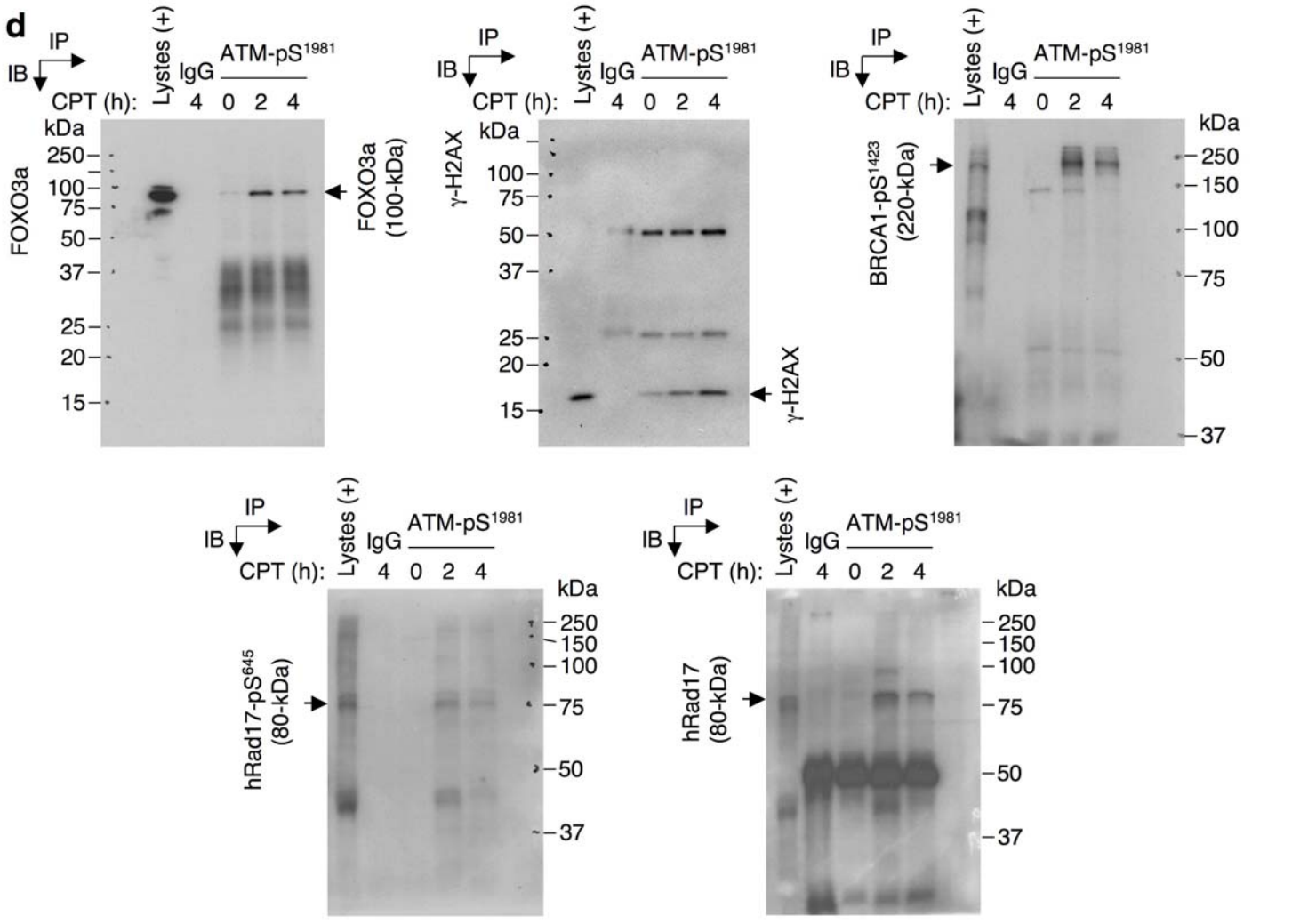


Tsai *et al.*, NCB-H11173C

Fig. S6 (full gels)

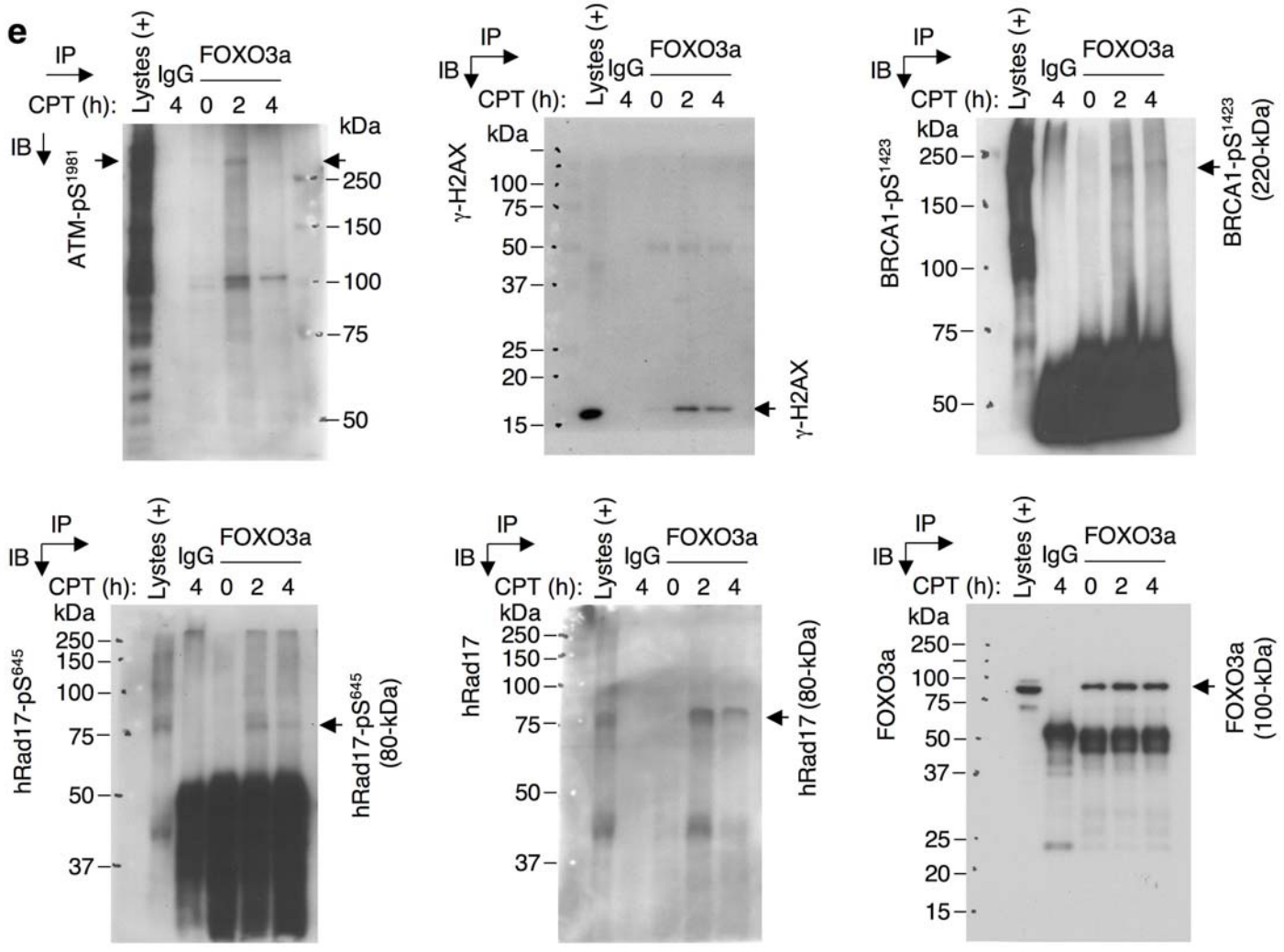


Tsai *et al.*, NCB-H11173C

Fig. S6 (full gels)

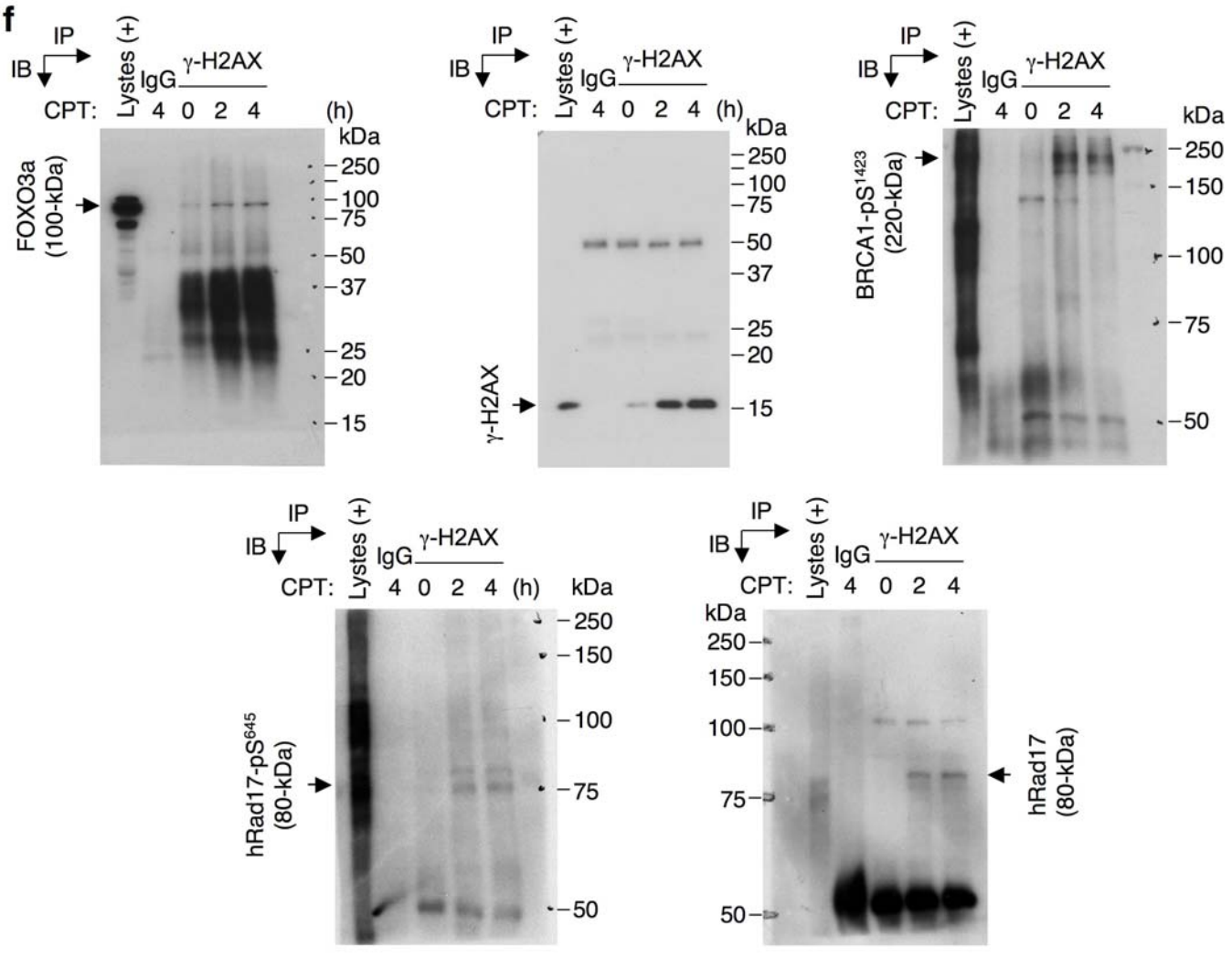


Tsai *et al.*, NCB-H11173C

Fig. S6 (full gels)

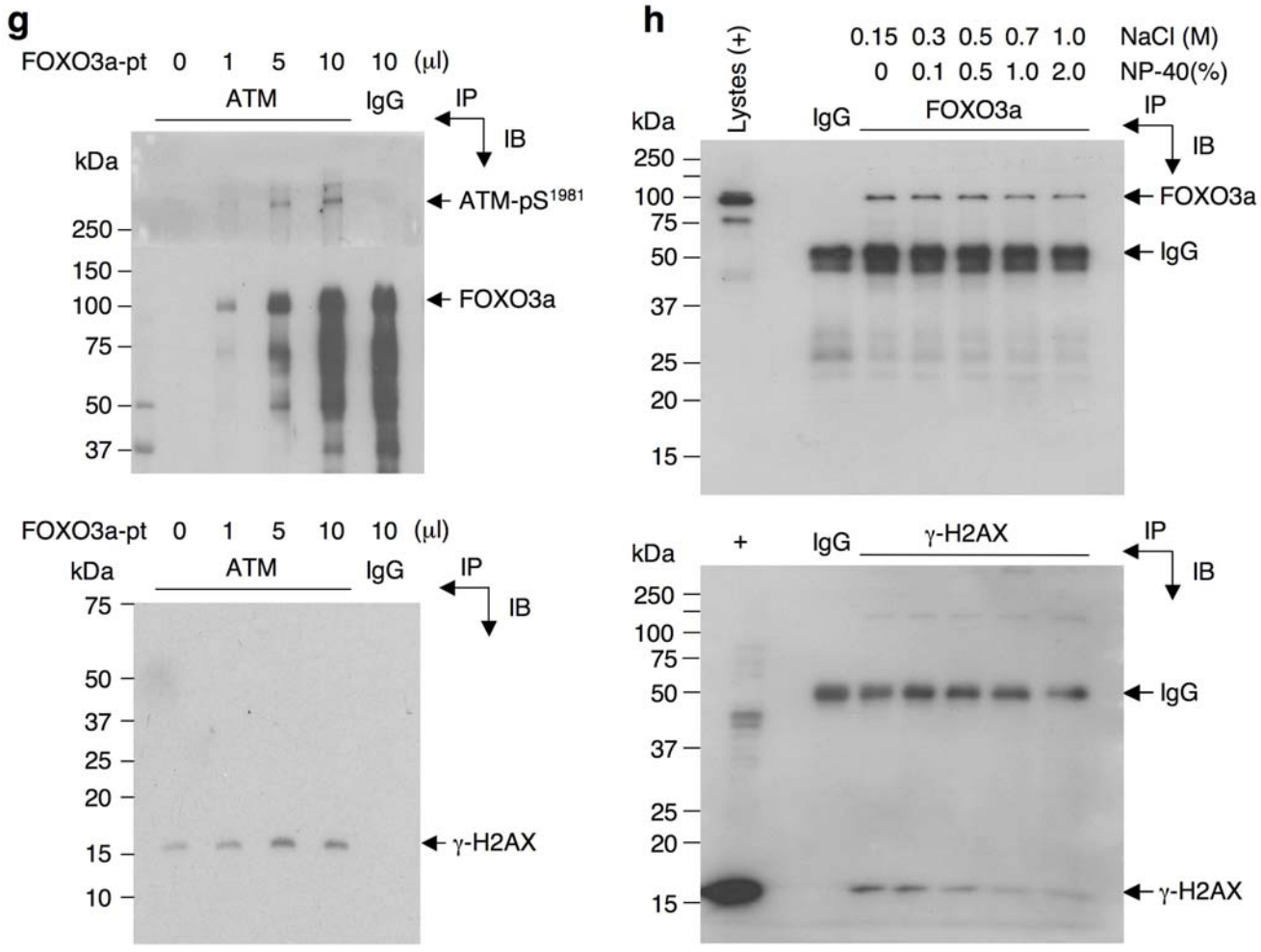


Tsai *et al.*, NCB-H11173C

**Legends for Supplementary Figures**

**Figure S1.** Silencing FOXO3a results in defective intra-S-phase and $G_2$/M phase cell-cycle checkpoints and FOXO3a plays a crucial role in activation of the ATM-response pathway after DNA damage. (**a**) Establishment of MCF-7 stable cell lines with FOXO3a downregulated (MCF7-Fd) or overexpressed (MCF7-FO) and control (MCF7-Cv). MCF-7 cells were infected with retroviruses expressing shRNA directed against human FOXO3a, or expressing HA-FOXO3a or control vectors. After puromycin selection, MCF7-Fd individual clones (Fd-1, Fd-25, Fd-35) or pooled clones (Fd-Pa and Fd-Pc), and MCF7-FO individual clones (FO33 and FO41), and vector control clones (Cv-4, Cv-14, and C12) were selected. The expressions of FOXO3a and p27Kip1 (a transcriptional target of FOXO3a) were determined by immunoblotting (IB) analysis with an antibody (Ab) against FOXO3a or p27Kip1 or β-actin (loading control). (**b**) Establishment of LNCaP stable cell lines with FOXO3a downregulated (LNCaP-Fd) or overexpressed (LNCaP-FO). The expressions of FOXO3a and p27Kip1 were determined as described above. (**c**) Analysis of the IR-induced intra-S-phase checkpoint. MCF-7 and MCF7-Fd-Pc cells were either untreated or treated with various doses of IR, incubated for 1 h at 37°C, then labeled with BrdU for 30 min at 37°C before fixation. DNA synthesis in replication was determined by flow cytometry. (**d**) LNCaP and LNCaP-Fd cells were either untreated or treated with various doses of IR as indicated. DNA synthesis was measured. (**e**) Analysis of the G2/M DNA damage checkpoint. MCF-7 cells with relatively high levels of FOXO3a (MCF7-Cv-4 and MCF7-FO33) and individual cell clones with relatively low levels of FOXO3a (MCF7-Fd-1, MCF7-Fd-25, and MCF7-Fd-35) were treated with camptothecin (CPT) (1μM) or control (DMSO) for 1 h. Cells in mitosis were determined by staining with an Ab against phosphorylated histone H3 at Serine-10 (P-H3) or an isotype IgG (negative control),

followed by Alexa 488 (green)-conjugated secondary Ab and propidium iodide (PI). The percentage of P-H3-positive cells was determined by flow cytometry. (**f**) A histogram shows the changes in percentage of P-H3-positive cells between CPT treatment and control that are the averages of 3 independent experiments from each cell line. (**g**) MCF7-FO33 and MCF7-Fd-35 cells were irradiated with 10 Gy or untreated (0 Gy) for 1 h, stained with an antibody against P-H3, and the percentage of P-H3-positive cells was assessed. (**h**) A histogram shows the changes in percentage of P-H3-positive cells between IR treatment and control that are the averages of 3 independent experiments. (**i**) LNCaP-FO and LNCaP-Fd cells were treated with CPT (1 μM) or control for 1 h, stained with an antibody against P-H3, and the percentage of P-H3-positive cells was determined. (**j**) LNCaP-FO and LNCaP-Fd cells were irradiated with 10 Gy or untreated (0 Gy) for 1 h, stained with an Ab against P-H3, and the percentage of P-H3-positive cells was assessed. The changes in percentage of P-H3-positive cells between treatment (CPT or IR) and control shown in histograms represent the averages of 3 independent experiments. (**k**) The role of FOXO3a in phosphorylation of ATM induced in cells treated with CPT. MCF-7, MCF7-FO33, and MCF7-Fd-Pa, and MCF7-Fd-Pc cells were treated with CPT (1 μM) or control for indicated times, and fixed. Cells were stained with an Ab specific to phospho-Serine-1981 of ATM (ATM-pS1981) or an isotype IgG (control), followed by Alexa 488-conjugated secondary Ab. The percentage of increase of the ATM-pS1981-positive population was determined by flow cytometry. (**l**) The role of FOXO3a in phosphorylation of H2AX induced in cells treated with CPT. MCF-7, MCF7-FO33, and MCF7-Fd-Pa, and MCF7-Fd-Pc cells were treated with CPT (1 μM) or control for indicated times, and fixed. Cells were stained with an Ab specific to phospho-Serine-139 of H2AX (γ-H2AX) or an isotype IgG (control), followed by Alexa 488-conjugated secondary Ab. The percentage of increase of the γ-H2AX-positive population was

determined by flow cytometry. (**m, n**) The results obtained by flow cytometry were confirmed in MCF-7 transfected with siRNA targeting FOXO3a or luc (control), and in MCF7-Fd-Pc cells after treated with IR (5Gy) or untreated (0Gy) for 5 min or 10 min by IB with Abs against FOXO3a, p27Kip1, ATM-pS1981, γ-H2AX or other proteins as indicated or β-actin (loading control).

**Figure S2.** Phosphorylation of S1981-ATM and its downstream mediators could be induced shortly after DNA damage. (**a**) MCF-7 cells were treated with IR (5 Gy or 3 Gy) for a short time course (i.e., 5, 10, 20, 30 min), and the levels of ATM-pS1981 and the other phospho-proteins in cytoplamic (Cyt.) and nuclear (Nuc.) extracts from these cells were subjected to immunoblotting (IB) analysis with specific phospho-antibodies (Abs) as indicated. As an expression control, the level of total expression of each protein was examined by IB with an Ab against whole protein as indicated. Abs against tubulin and PCNA were included as loading controls for Cyt. and Nuc. extracts, respectively. (**b**) MCF-7 cells were treated with IR (3 Gy) for a short time course and the levels of ATM-pS1981 and the other phospho-proteins in Cyt. and Nuc. extracts from these cells were assessed. (**c**) MCF-7 cells were treated with CPT (20 μM) for a short time course and the levels of ATM-pS1981 and the other phospho-proteins in Cyt. and Nuc. extracts from these cells were determined. (**d**) LNCaP cells were treated with IR (5 Gy) for a short time course and the levels of ATM-pS1981 and the other phospho-proteins in Cyt. and Nuc. extracts from these cells were determined. (**e**) Neither NEMO nor IKK is involved in the FOXO3a-mediated activation of the ATM DNA damage response. LNCaP cells were treated with IR (10 Gy) for a short time course (up to 60 min), and the levels of ATM-pS1981, NEMO phosphorylated at serine-85 (NEMO-pS85), NEMO, IKKα/β, and other

proteins as indicted in Cyt. and Nuc. extracts from these cells were examined. (**f**) The same IB analyses were performed with Cyt. and Nuc. extracts prepared from MCF-7 cells treated with CPT using Abs against ATM-pS1981, NEMO-pS85, NEMO, IKKα/β, and other proteins as highlighted. (**g**) As a vehicle control, IB analyses were carried out with whole lysates from MCF-7 cells treated with DMSO for various times using Abs as indicated.

**Figure S3.** FOXO3a may play an important role in the formation of γ-H2AX and ATM-pS1981 nuclear foci in response to DNA damage, the DNA damage-induced co-localization of FOXO3a with γ-H2AX or ATM-pS1981 is independent of the PI3K-Akt pathway, and co-localization of FOXO3a with ATM-pS1981 or γ-H2AX is also observed in human primary prostate tumour tissues *in vivo*. (**a**) MCF-7 cells were treated with IR (5 Gy) or untreated (0 Gy) for 10 min, fixed, and the subcellular localizations and co-localization of endogenous FOXO3a and γ-H2AX were detected using antibodies (Abs) against FOXO3a and γ-H2AX and followed by an Alexa Fluor 546 (red)- or Alexa Fluor 488 (green)-conjugated secondary Ab, respectively, and fluorescence microscopy. A nuclear stain 4',6-diamidino-2-phenylindole (DAPI) was used to show the nuclei, and co-localization of nuclear FOXO3a with γ-H2AX was shown as the merged images. An average (% Merge) of ~500 cells with co-localized nuclear FOXO3a and γ-H2AX on 3 independent slides was shown on the right panel. (**b**) The subcellular localizations and co-localization of endogenous FOXO3a and ATM-pS1981 in the same MCF-7 cells treated with CPT or DMSO were detected using antibodies against FOXO3a and ATM-pS1981. (**c**, **d**) The higher power views of γ-H2AX and ATM-pS1981 nuclear foci in MCF-7 cells treated with CPT (**a**, **b**) were shown. (**e, f**) The representative pictures of Fig. 2c and 2d. MCF-7 cells were transfected with siRNA targeting FOXO3a (si-FOXO3) or control, treated with CPT or DMSO

for 10 min, and then the subcellular localizations and co-localization of endogenous FOXO3a and γ-H2AX or ATM-pS1981 were detected using Abs against FOXO3a and γ-H2AX. A nuclear stain DAPI was used to show the nuclei, and co-localization of nuclear FOXO3a with (**e**) γ-H2AX or (**f**) ATM-pS1981 was shown as the merged images. The averages of >300 cells with γ-H2AX or ATM-pS1981 nuclear foci on 3 independent slides are shown in Fig. 2c and 2d. (**g, h**) The higher power views of γ-H2AX and ATM-pS1981 nuclear foci in MCF-7 cells treated with CPT and control-siRNA (**e, f**) are shown. (**i**) MCF-7 cells were treated with LY294002 (20 μM) plus IR (5 Gy) or untreated (0 Gy) for 10 min, fixed, and the sub-cellular localizations and co-localization of endogenous FOXO3a and γ-H2AX were detected using Abs against FOXO3a and γ-H2AX and followed by secondary Abs. DAPI was used to visualize the nuclei, and co-localization of nuclear FOXO3a with γ-H2AX was shown as the merged images. (**j**) The percentage of quantitative co-localization of FOXO3a with γ-H2AX was calculated using NIH ImageJ (v. 1.39f) software with the co-localization program. An average of 50 merged nuclear foci on 3 independent slides was determined. The results presented are the mean ± SEM. (**k**) The subcellular localizations and co-localization of endogenous FOXO3a and ATM-pS1981 in the same MCF-7 cells treated with LY294002 plus IR (5 Gy) or untreated (0 Gy) for 10 min were detected using Abs against FOXO3a and ATM-pS1981 and followed by secondary Abs. (**l**) The percentage of quantitative co-localization of FOXO3a with ATM-pS1981 with the co-localization program. (**m, n**) Human primary prostate tumour tissues (T) and normal tissues were stained with Abs against FOXO3a and ATM-pS1981 or γ-H2AX and followed by an Alexa Fluor 546- and Alexa Fluor 488-conjugated secondary Abs, respectively, and fluorescence microscopy. Co-localization of nuclear FOXO3a with (**m**) ATM-pS1981 or (**n**) γ-H2AX was shown as the merged images. (**o**, **p**) As controls, CPT did not affect the

immunofluorescence studies. (**o**) MCF-7 cells were treated with CPT (20 μM) for 10 min, stained with Abs against FOXO3a and ATM-pS1981, and followed by an indicated secondary Ab. Co-localization of nuclear FOXO3a with ATM-pS1981 was shown as the merged images. (**p**) MCF-7 cells were treated with CPT (20 μM) for 10 min without staining with a secondary Ab. There is no fluorescence signal detected with the CPT treatment alone using the wavelengths for detecting Alexa Fluor 488 and Alexa Fluor 546 fluorescence. Cells are shown under bright field light microscopy (Bright). Scale bars are indicated.

**Figure S4.** FOXO3a is associated with ATM-pSer1981 and γ-H2AX in the nucleus in cells treated with CPT, FOXO3a promotes ATM autophosphorylation of S1981, and DNA is not involved in the interactions between FOXO3a and ATM-pS1981 or γ-H2AX. (**a**-**d**) Nuclear extracts of MCF-7 cells treated with CPT (20 μM) for 2 h or 4 h or untreated (0 h) were subjected to immunoprecipitation (IP) with an antibody (Ab) against (**a**) FOXO3a or (**b**) ATM-pS1981 or (**c**) γ-H2AX or (**d**) FOXO1a followed by immunoblotting (IB) analysis with an Ab against the indicated protein or an isotype IgG (negative control). (**e, f**) Similarly, cell lystates of wild-type (wt) MEFs and FOXO3a(-/-) MEFs treated with CPT (20 μM) for an indicated time were subjected to IP with an Ab specific to (**e**) ATM-pSer1981 (ATM-pS) or (**f**) γ-H2AX followed by IB analysis with an Ab against the indicated protein or the same Ab used for IP (IP control). These IP and IB experiments were repeated at least twice. (**g**) 293T cells were co-transfected with various amounts of Flag-FOXO3a expression vector and pCDNA3 (control) vector, and cell lystates were analyzed by IB with specific phospho-Abs as highlighted. As an expression control, the level of total expression of each protein was examined by IB with an Ab against whole protein as indicated or β-actin (loading control). (**h**) Similarly, the levels of

FOXO3a or ATM-pS1981 or ATM in cell lysates from Wt MCF-7, MCF7-C12, MCF7-FO33, and MCF7-FO41 cells were determined by IB with Abs as indicated. (**i**) *In vitro* immuno-complex kinase (ICK) assays were performed by incubating various amounts of Flag-FOXO3a protein (FOXO3a-pt), which were IP-ed using an anti-Flag Ab from lysates of 293T transfected with Flag-FOXO3a vector, with equal amounts of endogenous ATM protein complex obtained from MCF-7 by IP plus 50ng linear double-stranded DNA fragments in the absence or presence of 20 units of protein phosphatase (PPase) as indicated. The levels of ATM-pSer1981, ATM, and FOXO3a were determined by IB with Abs as indicated. (**j**) ICK assays with ATM as in **i** except with various doses of purified GST-FOXO3a or GST (negative control) recombinant protein, which is free of DNA, instead of Flag-FOXO3a protein precipitates. (**k**) Lysates of MCF-7 cells treated with CPT (20 μM) for 2 h were subjected to IP with an anti-FOXO3a Ab, treated or untreated with DNase (2U), and followed by IB with an Ab against ATM-pS1981 or γ-H2AX or FOXO3a (IP positive control)). Total lysate was included as a positive (+) control for IB. (**l**) The same lysates were subjected to IP with an anti-γ-H2AX Ab, treated or untreated with DNase (2U), and followed by IB analysis with Abs as indicated. Total lysate was included as a positive (+) control for IB. (**m**) The same lysates were subjected to IP with an anti-FOXO3a Ab, treated or untreated with EtBr (10 μg/ml), and followed by IB with specific Abs. Total lysate was included as a positive (+) control for IB. (**n**) The same lysates were subjected to IP with an anti-γ-H2AX Ab, treated or untreated with EtBr (10 μg/ml), and followed by IB with specific Abs. Total lysate was included as a positive (+) control for IB. (**o-r**) The existence of large FOXO3a and ATM-pS1981 protein complexes in cells after DNA damage. (**o**) Lysates of MCF-7 treated with CPT (20 μM) for 2 h were subjected to size selection with a 100-kDa molecular weight cut-off column (Centricon-100, Millipore Corporation) by centrifugation at

5000×g for 1 h. The lysate retente in the spin column was subjected to IP with an anti-ATM-pS1981 Ab, and followed by IB with an Ab against FOXO3a or ATM-pS1981 (IP control). (**p**) The same IP samples were analyzed by IB with an Ab against Rad50 or ATM-pS1981 (IP positive control). (**q, r**) As protein size controls, the same lysate retente described in **o** was analyzed by IB with Abs against KU86 (86-kDa) (**q**) and PTEN (54-kDa) (**r**), respectively. The results indicate that the majority of medium size (below 100-kDa such as Ku86 and PTEN) proteins were excluded from the lysate retente of MCF-7 lysates.

**Figure S5.** The FOXO3a**-**mediated repair of damaged DNA *in vivo* was assessed by the quantitative real-time PCR (qPCR) and standard PCR amplification in the linear range or luciferase assays, and phosphorylation of ATM-pS1981, γ-H2AX, BRCA1-pS1423 and hRad17-pS645 can be induced upon DNA damage in a Gadd45a-independent manner. (**a**) MCF7-C5 and MCF7-FO33 cells were co-transfected with a circular pGL2-Basic (pGL2-B) DNA vector pre-damaged by nicking endonucleases and an undamaged pGEX-5X-3 (pGEX) vector. At 48 h after transfection, total low-molecular weight DNA was selectively isolated and the repair of damaged DNA was assayed by qPCR using specific primers for pGL2-B and pGEX. The relative copies of repaired template were calculated by the ratio between qPCR product quantities derived from pGL2-B and those obtained from the corresponding pGEX. The results presented represent the mean of three independent experiments with duplicated samples. (**b**) The repair of damaged DNA as described in **a** was assayed by standard PCR amplification in the linear range using specific primers for pGL2-B [within the luciferase (Luc) gene] and pGEX templates (5 ng of DNA/each reaction) (full gels are shown). (**c**) The same PCR reactions as described in **b** were performed with various amounts of DNA templates as

indicated (a dose response) to show that the PCR products obtained in **b** were indeed within the linear range of PCR amplification. The units of mean PCR intensities are based on arbitrary unit values. (**d**) The images show full gels of the products derived from PCR amplification as described in **c**. The amounts of DNA templates used in **b** were indicated with arrows. (**e, f**) Similarly, wt MEFs and FOXO3a(-/-) MEFs were co-transfected with a damaged p27-Luc vector and an undamaged pGEX vector. The repair of damaged DNA was assayed by standard PCR amplification in the linear range using specific primers for p27-Luc [within the Luc gene] and pGEX (10 ng of DNA/each reaction) (full gels are shown). (**g**) The same PCR reactions as described in **e** and **f** were performed with various amounts of DNA templates as indicated (a dose response) to show that the PCR products obtained in **e** and **f** were indeed within the linear range of PCR. The units of mean PCR intensities are based on arbitrary unit values. (**h**) The images show full gels of the products derived from PCR as described above in **g**. The amounts of DNA templates used in **f** were indicated with arrows. (**i**) MCF7-C5 and MCF7-Fd-25 were co-transfected with either a *Hind*III-cut FRE-Luc reporter vector (the link between the promoter and the Luc gene was disengaged so that it should not display any transcriptional activity if the double-strand DNA breaks are not repaired *in vivo*) or a *Sal*I-linearized FRE-Luc vector (the promoter is still linked to the Luc gene properly so that its transcription should be functional) (1 μg) together with an intact pRL-TK plasmid (0.1 μg) for normalization. At 24 h after transfection, Luc assays were performed, and the data presented represent the mean of three independent experiments. (**j**) The role of FOXO3a in the repair of damaged DNA occurred *in vivo*. MCF-7 and MCF7-Fd-Pc were transfected with FRE-Luc (firefly Luc) reporter (1 μg) followed by treatment with CPT for 4 h to induce DNA damage *in vivo*. The relative firefly Luc activity was normalized by a second transfection with an undamaged TK-renulla Luc (pRL-TK)

plasmid (0.1 μg) after removal of CPT in culture. At 24 h after transfection, Luc assays were performed, and the relative Luc activities presented represent the mean of three independent experiments. (**k**) Wt Gadd45a(+/+) MEFs and Gadd45a(-/-) MEFs were treated with IR (10 Gy), and single-cell electrophoresis was carried out 1 h after IR, and the relative comet tail moment was determined. A histogram shows the average of three independent experiments. (**l**) Wt MEFs and Gadd45a(-/-) MEFs were co-transfected with either a *Hind*III-cut FRE-Luc or a *Sal*I-linearized FRE-Luc reporter vector (1 μg) together with an intact pRL-TK plasmid (0.1 μg). At 24 h after transfection, Luc assays were performed, and the data presented show the average of three independent experiments. Phosphorylation of ATM-pS1981 and its downstream targets can be induced upon DNA damage in a Gadd45a-independent manner. (**m**) MCF-7 cells transfected with siRNA targeting Gadd45a or Luc (control) were treated with CPT or DMSO (control) for 2 h. Total lysates of the treated cells were subjected to IB analysis with the indicated Abs or anti-β-actin (loading control). (**n**) Wt LNCaP and LNCaP-Fd were treated with CPT or DMSO. Total lysates of the treated cells were subjected to IB analysis. (**o**) Wt MEFs and Gadd45a(-/-) MEFs were treated with IR (10 Gy) for 1 h. Total lysates of the treated cells were subjected to IB analysis.

**Figure S6.** The candidate protein domains and sequence motifs involved in the interaction between FOXO3a and ATM, and confirmation of antibody specificity by full gel immunoblotting (IB) and the stringency control of immunoprecipitation (IP). (**a**) A diagram depicts the relative positions of GST-FOXO3a (GST-FO) fusion proteins in the entire carboxy-terminal region of FOXO3a (301-673). The dark green color highlights a candidate GST-FO(579-625) fragment that interacts with ATM strongly in GST-pull down assays. (**b**) The

conserved sequence motifs within the candidate 8 amino acids (a.a.) of FOXO3a(616-623) fragment that interacts with ATM as shown in Figure 5c-e. The conserved Leucine (L), Cysteine (C), and aspartic acid (D) residues among the FOXO family (FOXO3a, FOXO1a, and FOXO4) are boxed and highlighted with blue color. The specific mutated amino acids in the mutant GST-FO(616-623) clones are shown in red colors, where C and D residues were mutated to alanine (A), and L was mutated to glycine (G). (**c**) A diagram shows the relative positions of GST-ATM fusion proteins in human ATM protein (a.a.1-3056). The various GST-ATM(1-247), (250-522), (523-769), (772-1102), (1098-1371), (1245-1435), (1439-1770), (1764-2138), (2141-2428), (2427-2841), and (2682-3012) recombinant proteins were generated as described[S19]. The candidate domain (a.a.1764-2841) of ATM that interacts with FOXO3a is shown in yellow color and the putative "FAT" domain (a.a.1960-2566)[25] is depicts in red color. The autophosphorylation site S1981 within the FAT domain of ATM is also highlighted. (**d**) Nuclear extracts of MCF-7 treated with CPT were subjected to IP with an Ab against ATM-pS1981 followed by IB with an indicated Ab or an isotype IgG (control) (a repeat of Fig. 3d). (**e**) Nuclear extracts of MCF-7 cells treated with CPT (20 μM) for 2 h or 4 h or untreated (0 h) were subjected to IP with an anti-FOXO3a antibody (Ab) followed by whole-gel IB analysis with an indicated Ab or an isotype IgG (control) (a repeat of Fig. 3c). (**f**) Nuclear extracts of MCF-7 cells treated with CPT were subjected to IP with an Ab against γ-H2AX followed by IB with an indicated Ab or an isotype IgG (control) (a repeat of Fig. 3e). (**g**) *In vitro* kinase assays were performed with various amounts of FOXO3a protein and endogenous ATM protein complex. The levels of phosphorylated ATM (ATM-pS1981, FOXO3a, and γ-H2AX were determined by IB with the indicated Abs (the images of full gels show repeats of key Abs in Fig. 3f). (**h**) The stringency control of IP of Fig. 3. To demonstrate the specificity of IP, some immunoprecipitates

were also subjected to high stringency washes in cell lysis buffer (pH 7.4) containing various concentrations (0.15, 0.3, 0.5, 0.7, or 1 M) of NaCl in conjunction with various amounts (0, 0.1, 0.5, 1, or 2 %) of NP40 as indicated. After washing, immunoprecipitates were subjected to IB analysis. Two images show representative stringency controls of IP with anti-FOXO3a in Fig. 3c, and with anti-γ-H2AX in Fig. 3e. All IP/IB experiments were repeated at least twice.

**Supplementary Text**

Our findings may define an important role for FOXO3a in regulating the formation of γ-H2AX and ATM-pS1981 nuclear foci, promoting ATM autophosphorylation and repair of damaged DNA. It should be noted that CPT can exhibit blue fluorescence with an excitation wavelength of 360 nm (UV light) and an emission wavelength of 430 nm[S1,S2]. The excitation (Ex) wavelength and emission (Em) wavelength of CPT are far away from those of Alexa Fluor 488 (Ex 495/Em 519)- and Alexa Fluor 546 (Ex 556/Em 573)-conjugated secondary antibodies used in our immunofluorescence studies. Thus, CPT should not affect our immunofluorescence studies. To verify this point, we showed that there was no fluorescence signal detected with the CPT treatment alone using the wavelengths for Alexa Fluor 488 and Alexa Fluor 546 (Supplementary Fig. S3o,p). In fact, the CPT-induced immunofluorescence studies have been extensively reported in the literature[S3-S6].

To demonstrate that these large FOXO3a-ATM protein complexes exist in cells after DNA damage, we tested the associations among FOXO3a, ATM-pS1981, and γ-H2AX in lysates of MCF-7 cells treated with CPT by using the same IP/IB approach but pretreating the lysates with a 100-kDa molecular weight cut-off column (Centricon-100, Millipore Corp.) to exclude medium-sized proteins or proteins smaller than 100 kDa such as Ku86 (86-kDa) and PTEN (54-kDa). Interestingly, our results showed that the originally observed interactions among FOXO3a, ATM-pS1981, and γ-H2AX in these lysates were retained—and in fact they were strengthened through the enrichment of large proteins in the lysates (Supplementary Fig. S4k-n), confirming that these large FOXO3a/ATM-pS1981 or FOXO3a/γ-H2AX protein complexes did indeed exist in the cell lysates.

To confirm that FOXO3a promoted the repair of double-stranded DNA breaks, we transfected MCF7-C5 and MCF7-Fd-25 cells with either an endonuclease-cut FRE-Luc reporter (+*Hind*III), in which the promoter containing the FOXO-responsive elements (FRE) was disengaged from the Luc gene, or a linearized FRE-Luc (+*Sal*I) that did not alter the link between its promoter and the Luc gene as control in a modified host-cell reactivation assay[24]. The damaged Luc reporter should not display any transcriptional activity if it is not repaired *in vivo*. We showed that silencing FOXO3a in MCF7-Fd-25 cells significantly reduced reactivation of the promoter-disrupted FRE-Luc reporter (+*Hind*III) (Supplementary Fig. S5i). To further verify the role of FOXO3a in the repair of damaged DNA that occurs in living cells, we used a similar host-cell reactivation assay as follows. We transfected MCF-7 and MCF7-Fd-Pc cells with FRE-Luc followed by treatment with CPT for 4 h to induce DNA damage. Indeed, we found that the relative Luc activity was reduced in MCF7-Fd-Pc cells after exposure to CPT as compared with that in MCF-7 cells (Supplementary Fig. S5j). These results suggest that increasing FOXO3a promotes the repair of damaged DNA.

Because our findings indicate that most of the unphosphorylated ATM and H2AX was present in the nucleus (Supplementary Fig. S2a-e), it is plausible that FOXO3a may activate phosphorylation of ATM inside the nucleus, assuming that ATM undergoes autophosphorylation and H2AX is phosphorylated by the activated ATM-pS1981 kinase upon DNA damage. We did detect a low but not negligible amount of FOXO3a in the nucleus before DNA damage (Supplementary Fig. S2a-e), where FOXO3a presumably associates with chromatin DNA and does not bind ATM directly (Fig. 3c,d).

Evidence is emerging to indicate that activation of ATM is induced by the MRN complex, which binds and unwinds the broken DNA ends and recruits ATM to sites of DNA

breaks in an ATM autophosphorylation-independent manner[6,9]. It is plausible that FOXO3a may trigger ATM autophosphorylation upon DNA damage and cooperate with the MRN complex or other mediators to recruit activated ATM-pS1981 to sites of DNA breaks, leading to the initiation of the DNA repair program. Interestingly, an interaction between ATM and NEMO may regulate NF-kB signaling in response to genotoxic stimuli[20]. If NEMO was being phosphorylated by ATM in LNCaP or MCF-7 cells after IR or CPT exposure under our experimental conditions, then NEMO-pS85 and ATM-pS1981 would be exported from the nucleus to the cytoplasm[20]. However, our results clearly indicate that neither NEMO nor IKK is involved in the FOXO3a-mediated activation of ATM. The differences between our findings and those of Wu et al.[20] after IR can be attributed to the different time courses of the experiments (our detection sooner after IR vs. their measurements later times after IR) or to the different cell types used (our MCF-7 and LNCaP cells vs. their murine pre-B cell line 1.3E2 or others), in which the expression or the role of NEMO may be different.

Although the domain of FOXO3a binding to ATM appears to be conserved among FOXO members, the function of FOXO3a could not be supplemented by other members (FOXO1a or FOXO4) because the expression level of FOXO1a or FOXO4 was very low as compared to that of FOXO3a in MCF-7 and LNCaP cells (Supplementary Fig. S2a,d). Furthermore, our results showed that the levels of FOXO1a and FOXO4 were not induced after IR 5Gy for 30 min while the level of FOXO3a was significantly increased in the nucleus upon IR 5Gy after 5 min (Supplementary Fig. S2a), suggesting that FOXO3a is the primary FOXO member activated by IR at early stages in these cells. The members of FOXO subfamily are conserved in structure and function; however, the FOXO3a-knockout mice data indicate that certain indispensable functions of FOXO3a could not be constituted by other members

(FOXO1a or FOXO4)[S7,S8], suggesting that loss of certain essential function of FOXO3a could have a dramatic effect on biological phenotypes. It has been recently found that FOXO1a is an ATM substrate[S9]. However, it is unknown whether or not FOXO3a or FOXO4 will be a substrate of ATM. If FOXO3a is a potential substrate of ATM, it is plausible that FOXO3a can still be up and downstream of ATM through a novel feedback mechanism. This kind of feedback mechanism has been discovered and well established in certain critical signaling networks. For instance, it has been demonstrated that Mre11, Rad50, and Nbs1 (MRN) are not only downstream targets of ATM (ATM substrates)[S10-S12] but also act upstream, via protein-protein interaction, promoting optimal ATM activation[S13-S16]. Although it is possible that FOXO might be de-activated by DNA damage via Akt phosphorylation, Akt has been shown to be activated by IR weakly approximately 20 min after IR[S17,S18]. Consistent with these reports, we showed that p-Akt-Ser473 (an activated Akt) was only weakly induced in the cytoplasm, but not in the nucleus, at ~20 min after IR (Supplementary Fig. S2a). Since phosphorylation of ATM-pS1981 can be induced in the nucleus shortly after DNA damage (5 min after IR or CPT) (Suppl Fig. S2a-e), the effect of FOXO3a on ATM activation in the nucleus occurred prior to a very weak activation of Akt in the cytoplasm after IR. Although FOXO could potentially be de-activated by Cdk2, it has been shown that IR reduces Cdk2-mediated FOXO1 phosphorylation, resulting in FOXO1 activation[S4]. In other words, FOXO could be activated by DNA damage via inhibition of Cdk2. Collectively, these reports and our results suggest that FOXO3a should not be significantly de-activated by IR via Akt and Cdk2 phosphorylation at early stages of the response to IR. In addition, we observed the uneven ATM bands relative to control in our ATM GST pull-down data (Fig. 5a-e). Because the FOXO-bound ATM is separated from the GST-FOXO-ATM protein complex, it is conceivable that the viscosity of the loading buffer

containing the mixture of GST-FOXO-ATM protein complex could be relatively higher than that of the same loading buffer containing a small amount of total lysate (positive control). Furthermore, since it is necessary to analyze the high-molecular weight ATM proteins (~370 kDa) on low percentage (such as 6% gel) SDS-PAGE, it is relatively common to observe ATM bands that are not on the same line on immunoblots.

To exclude the possibility of that the growth arrest and DNA-damage-inducible protein 45a (Gadd45a)[23] is involved in the observed FOXO3a-mediated repair of damaged DNA, we carried out the same comet assay and host-cell reactivation Luc assay as described above. Our results showed that the extent of repair of damaged DNA remained the same in Gadd45a(-/-) MEFs and in wt Gadd45a(+/+) MEFs after IR in a comet assay or after transfection with the pre-damaged Luc DNA in the Luc assay (Supplementary Fig. S5k,l). Furthermore, we also found that the amounts of BRCA1-pS1423 and hRad17-pS645 that were induced paralleled the amounts of ATM-pS1981 induced in wt and Gadd45a-knockdown MCF-7 and LNCaP cells after CPT treatment (Supplementary Fig. S5m,n). Similarly, the amounts of BRCA1-pS1423 that were induced paralleled the amounts of ATM-pS1981 induced in wt and Gadd45a(-/-) MEFs after IR (10Gy) (Supplementary Fig. S5o), confirming that phosphorylation of BRCA1-pS1423 and hRad17-pS645 can be induced after DNA damage in a Gadd45a-independent manner. Collectively, these new findings suggest that the observed promotion of DNA damage repair is not mediated through Gadd45a but rather is a direct effect of increased FOXO3a levels.

**Supplementary Materials and Methods**

**Plasmid constructs**

For mammalian two-hybrid assays: pACT-FOXO3a-FL, pACT-FO(301-673), and pACT-FO(301-623) mutants clones were created by subcloning a *BamH*I/*Sal*I fragments from pGEX-FOXO3a, pGEX-FO(301-673), and pGEX-FO(301-623) mutant constructs into the *BamH*I/*Sal*I site of pACT (Promega Corp., Madison, WI), respectively. pBIND-ATM(1802-2571) was constructed by PCR followed by sequential subclonings. The ATM(1802-2571) fragment was generated by PCR using pCDNA3-Flag-ATM (kindly provided by M. Kastan) as a template, the primers 5'-GTCGACAAAATCATGACATTT-GGATAAAGAC-3' (containing the *Sal*I site) and 5'-GCGGCCGCTTCATCTCTGTTTGC-ATTTGCTAA-3' (containing the *Not*I site) and Pfu turbo DNA polymerase (Stratagene, CA). The PCR reaction was incubated at 72 $^{o}$C for 10 min in the presence of 0.05 units/μl of Taq DNA polymerase (Eppendorf, Hamburg, Germany), and the ATM(1802-2571) PCR fragment was cloned into pCR2.1-TOPO vector (Invitrogen, CA). This pCR-TOPO-ATM(1802-2571) construct was then digested with *Sal*I/*Not*I and subcloned into the *Sal*I/*Not*I sites of pBIND (Promega). For GST pull-down assays: the various GST-fusion FOXO3a plasmids were constructed by subcloning of the DNA fragments containing the specific domain of FOXO3a [GST-FO-(1-301), (301-673), (301-346), (347-392), (393-439), (440-485), (486-531), (532-578), (579-625), and (626-673)] into a GST expression vector (pGEX-5X-3, , Amersham) using the PCR technique as described[14]. The GST-FO-(579-588), (589-597), (598-606), (607-615), (616-625), and (610-623) fusion constructs were generated by subcloning of the duplex oligonuceotides corresponding to the specific regions of FOXO3a and their sequences are listed below.

FO-(579-588): 5'-TCGACTCTATGCAAACCCTCTCGGACTCTCTCTCAGC-3' and

5’-GGCCGCTGAGAGAGAGTCCGAGAGGGTTTGCATAGAG-3’

FO-(589-597): 5’-TCGACGGCTCCTCCTTGTACTCAACTAGTGCAGC-3’ and

5’-GGCCGCTGCACTAGTTGAGTACAAGGAGGAGCCG-3’

FO-(598-606): 5’-TCGACAACCTGCCCGTCATGGGCCATGAGAAGGC-3’ and

5’-GGCCGCCTTCTCATGGCCCATGACGGGCAGGTTG-3’

FO-(607-615): 5’-TCGACTTCCCCAGCGACTTGGACCTGGACATGGC-3’ and

5’-GGCCGCCATGTCCAGGTCCAAGTCGCTGGGGAAG-3’

FO-(616-625): 5’-TCGACTTCAATGGGAGCTTGGAATGTGACATGGAGGC-3’ and

5’-GGCCGCCTCCATGTCACATTCCAAGCTCCCATTGAAG-3’

FO-(610-623): 5-TCGACGACTTGGACCTGGACATGTTCAATGGGAGCTTGGAATGTGACGC-3’

and 5’-GGCCGCGTCACATTCCAAGCTCCCATTGAACATGTCCAGGTCCAAGTCG-3’

The mutant GST-FO(616-623) plasmids were constructed by subcloning of the duplex oligonuceotides, and their sequences (the coding strand) are shown below.

FO-(616-623)L620*G*: 5’-TCGACTTCAATGGGAGCGGGGAATGTGACATGGAGGC-3’

FO-(616-623)C622*A*: 5’-TCGACTTCAATGGGAGCTTGGAAGCTGACATGGAGGC-3’

FO-(616-623)D623*A*: 5’-TCGACTTCAATGGGAGCTTGGAATGTGCCATGGAGGC-3’

FO-(616-623)CD-*AA*: 5’-TCGACTTCAATGGGAGCTTGGAAGCTGCCATGGAGGC-3’

FO-(616-623)LCD-*GAA*: 5’-TCGACTTCAATGGGAGCGGGGAAGCTGCCATGGAGGC-3’

The mutant GST-FO(301-623) plasmids were generated by the PCR cloning technique as described above, using FOXO3a cDNA as a template and the primers as shown below. The sense primer with the *Sal*I site for all 5 mutant FO(301-623) fragments is: 5’-TTTGTCGACGATGAGCTGGATGCGTGGACGG-3’, and the antisense primers with the *Not*I site for these mutant FO(301-623) fragments are:

FO-(301-623)L620*G*: 5’-TTTGCGGCCGCCTCCATGTCACATTCCCCGCTCCCATTGAAC-3’

FO-(301-623)C622*A*: 5’-TTTGCGGCCGCCTCCATGTCAGCTTCCAAGCTCCCATTGAAC-3’

FO-(301-623)D623*A*: 5'-TTTGCGGCCGCCTCCATGGCACATTCCAAGCTCCCATTGAAC-3'

FO-(301-623)CD-*AA*: 5'-TTTGCGGCCGCCTCCATGGCAGCTTCCAAGCTCCCATTGAAC-3'

FO-(301-623)LCD-*GAA*: 5'-TTTGCGGCCGCCTCCATGGCAGCTTCCCCGCTCCCATTGAA-CATGTC-3'. All mutations were confirmed by DNA sequencing.

The various GST-ATM (1-247), (250-522), (523-769), (772-1102), (1098-1371), (1245-1435), (1439-1770), (1764-2138), (2141-2428), (2427-2841), and (2682-3012) plasmids were kindly provided by K.K. Khanna (Queensland, Australia)[S19].

**siRNA transfection, FOXO3a(-/-) and Gadd45a(-/-) MEFs.** MCF-7 or LNCaP cells were transfected with specific small-interfering RNA (siRNA) targeting FOXO3a (si-FOXO3a) (5'-GAGCUCUUGG-UGGAUCAUC$_d$T$_d$T-3') or Gadd45a-siRNA (si-Gadd45a, obtained from Santa Cruz Biotechnology) or control luc siRNA (5'-CUUACGCUGAGUACUUCGA$_d$T$_d$T-3') duplex (Dharmacon) (4 μM/2x10$^6$ cells) by electroporation using Nucleofector 1 (amaxa) or Lipofectamine 2000 (Invitrogen Corp.), and lysates were prepared 48 h after transfection as described previously[14]. Wild-type (wt) and FOXO3a(-/-) MEF cells were kindly provided by R. Depinho[S7] and N. Motoyama[S8]. Gadd45a(-/-) MEFs and their control wt MEFs were kindly provided by A.J. Fornace Jr.[S20]. In general, MEF cells were derived from E14.5 embryos generated from normal control and FOXO3a-knockout mice, respectively, by the standard methods as described previously[S21].

**Polymerase chain reaction (PCR) DNA repair assay.** These assays were performed as described[23] with some modifications. MCF7-C5, MCF7-C12, and MCF7-FO33 cells were plated at a density of 4x10$^5$ cells in 12-well plates. To induce sufficient damages on circular plasmids in a controlled manner, pGL2-Basic (pGL2-B) DNA vector was irradiated with UV

at 5000J/m$^2$ (UV Stratalinker Model 2400, Stratagene) as described[23] or digested with nicking endonucleases *N.Alw*I and *N.BstNB*I (New England Biolabs, MA), which bind to 5-bases recognition sequences and cleave only one strand of DNA on a double-stranded DNA substrate. After digestion, the damaged pGL2-B vector remained as circular DNA, whereas the luciferase (Luc) gene of pGL2-B was nicked heavily on both strands of DNA so that it should not display any PCR product if the template DNA is not repaired *in vivo*. Cells were co-transfected with the pre-damaged pGL2-B and an undamaged pGEX 5X-3 (pGEX) vector by using Lipofectamine 2000 (Invitrogen Corp.) or FuGENE-6 (Roche). Forty-eight hours after transfection, total low-molecular weight DNA was selectively isolated by a modified Hirt extraction method using mini-prep spin columns as described[S22]. The repair of damaged DNA was assayed by the standard PCR method at linear range using specific primers for pGL2-B (5'-GTCACATCTCATCTACCTCC-CG-3' and 5'-GCGCCCCCAGAAGCAATTTCG-3') and pGEX (5'-CTGGCAAGCCA-CGTTTGGTG-3' and 5'-GGAGCTGCATGTGTCAGAGG-3'). The percentage of PCR amplification of repaired template was calculated by the ratio between the PCR product quantities derived from pGL2-B and those obtained from the corresponding pGEX. The results presented represent the mean of three independent experiments with duplicated samples. Similarly, wt MEFs and FOXO3a(-/-) MEFs were co-transfected with the pre-damaged pGL2-B and undamaged pGEX and assayed by PCR as described above.

**Quantitative real-time PCR**

Specific primers for the pGL2-basic vector were designed using Primer Express 1.5 (Applied Biosystems, CA). All quantitative real-time PCR analyses were performed on a Chromo4 Real

Time PCR Instrument (Bio-Rad Laboratories, CA). Each reaction included a 25-μl mixture containing 0.3 μM of each primer, 12.5 μl of iQ SYBR Green Supermix (Bio-Rad), and 20 pg of the extracted DNA from MCF-7 cells. Amplification was carried out at 95 °C for 10 min, followed by 40 cycles of denaturation at 95 °C for 15 sec, and annealing and extension at 60 °C for 1 min. Specificity of PCR was checked by analyzing melting curves and by gel electrophoresis of the amplicon. For normalization, pGEX was used. Standard curves were generated using serially diluted intact plasmids. The recovery of pGL2-basic was determined by (initial number of intact pGL2)/(initial number of pGEX). The primer pairs used were pGL2-F1: 5'-CTTCCATCTTCCAGGGATACGA-3'; pGL2-R1: 5'-GATTAACGCCCAGCGTTTTC-3'; pGL2-F2: 5'-CGGAAAACTCGACGCAAGA-3'; pGL2-R2: 5'-GCGTTTAAGGGCACCAATAACT-3'; pGEX-F: 5'-CATGGACCCAATGTGCCTG-3'; pGEX-R: 5'-GATCCGATTTTGGAGGATGGT-3'.

**Luciferase DNA repair assay.** These assays were performed as described[24] with some modifications using the damaged FRE-Luc reporter vector, in which a thymidine kinase (TK) promoter containing the FOXO-responsive elements (FRE) drives the transcription of a Luc gene. To introduce double-stranded DNA breaks to FRE-Luc whose promoter was disrupted from the Luc gene, FRE-Luc vector was digested with restriction endonuclease *Hind*III (New England Biolabs), which cuts the vector between the promoter and the Luc gene. Because the link between the promoter and the Luc gene was disrupted, it should not display any transcriptional activity if the double-strand DNA breaks are not repaired *in vivo*. As a control, FRE-Luc vector was digested with restriction endonuclease *Sal*I (New England Biolabs), which cuts the vector outside of the promoter and the Luc gene resulting in a linearized DNA containing a functional FRE-Luc transcriptional unit. MCF7-C5 and MCF7-Fd-25 cells were

co-transfected with either a *Hind*III-cut FRE-Luc vector or a *Sal*I-linearized FRE-Luc vector (1 μg) together with an intact TK-renilla-Luc (pRL-TK, Promega) reporter (0.1 μg) for normalization by using Lipofectamine 2000. Twenty-four hours after transfection, cell lysates were prepared and assayed for Luc activities with Dual-Luciferase Reporter Assay System (Promega). The transfection efficiency was normalized by renilla luc activity, and the data presented represent the mean of three independent experiments. Assays of the repair of damaged DNA that occurs *in vivo* were carried out as described above except using an intact FRE-Luc reporter for initial DNA transfection. MCF-7 and MCF7-Fd-Pc cells were plated at a density of $4x10^5$ cells in 12-well plates. On the next day, cells were transfected with undamaged FRE-Luc reporter (1 μg) using FuGENE 6 (Roche) followed by treatment with CPT (20 μM) for 4 h to induce DNA damage *in vivo*. Four hours after treatment, cells were washed twice with PBS to remove CPT, and transfected with an undamaged pRL-TK reporter (0.1 μg) using FuGENE 6. Twenty-four hours after the second transfection, cell lysates were prepared and assayed for Luc activities with Dual-Luciferase Reporter Assay System as described. The transfection efficiency was normalized by renilla luc activity, and the data presented represent the mean of three independent experiments.

**LY294002 treatment**

MCF-7 cells were treated with 20 μM LY294002 (an inhibitor for blocking the PI3K-Akt pathway) plus CPT (10 μM) or DMSO (control) for 2 h, the media were removed, and cells were fixed. Then, the treated cells were antibodies specifically against FOXO3a plus γ-H2AX or ATM-pS1981, followed by an Alexa Fluor 546 (red)- or Alexa Fluor 488 (green)-conjugated secondary antibody, respectively, and stained with a nuclear stain 4',6-diamidino-2-

phenylindole (DAPI). The subcellular localizations and co-localization of endogenous FOXO3a and γ-H2AX or ATM-pS1981 in the treated cells were visualized by fluorescence microscopy.

**Ethidium bromide (EtBr) and DNase treatments**

Lysates of MCF-7 cells treated with CPT (20 μM) for 2 h were subjected to immunoprecipitation (IP) with an anti-FOXO3a or anti-γ-H2AX antibody (Ab). After two washes with IP buffer, the precipitates were divided into two equal portions. One portion was treated with EtBr (10 μg/ml) for 5 or 10 min at room temperature and the other portion was not treated (control). After washing, both samples were subjected to immunoblotting (IB) analysis. The same lysates of MCF-7 cells were subjected to IP with an anti-FOXO3a or anti-γ-H2AX Ab. After washing, the precipitates were divided into two equal parts. One part was treated with Turbo-DNase (2 U, Ambion Inc.) for 2 or 10 min at room temperature and the other part was not treated (control). After washing, both samples were subjected to IB analysis. The absence of DNA contamination in the treated IP samples was verified by standard DNA agarose gel eletrophoresis followed by EtBr (10 μg/ml) staining.

**Protein size selection**

Lysates of MCF-7 cells treated with CPT (20 μM) for 2 h were subjected to size selection with a 100-kDa molecular weight cut-off column (Centricon-100, Millipore Corporation, MA) by centrifugation at 5000×g for 1 h at 4°C. The retente in the spin column was collected and used for subsequent immunoprecipitation and immunoblotting analysis.

**Supplementary References**

S1. Mu, L., Elbayoumi, T.A., & Torchilin, V.P. Mixed Micelles made of Poly(ethylene glycol)-Phosphatidylethanolamine Conjugate and D-α-tocopheryl Polyethylene Glycol 1000 Succinate as Pharmaceutical Nanocarriers for Camptothecin. *Int. J. Pharm.* **306(1-2)**, 142–149 (2005).

S2. Opanasopita, P. *et al*. Camptothecin-incorporating N-phthaloylchitosan-g-mPEG self-assembly micellar system: Effect of degree of deacetylation. *Colloids and Surfaces B: Biointerfaces* **60**, 117-124 (2007).

S3. Ohtsuka, T. *et al.* ASC is a Bax adaptor and regulates the p53-Bax mitochondrial apoptosis pathway. *Nat. Cell Biol.* **6**, 121-128 (2004).

S4. Huang, H., Regan, K. M., Lou, Z., Chen, J., & Tindall, D. J. CDK2-dependent phosphorylation of FOXO1 as an apoptotic response to DNA damage. *Science* **314**, 294-297 (2006).

S5. Zhang, Y.-W. *et al.* Genotoxic Stress Targets Human Chk1 for Degradation by the Ubiquitin-Proteasome Pathway. *Mol. Cell* **19**, 607-618 (2005).

S6. Chowdhury, D. *et al.* γ-H2AX Dephosphorylation by Protein Phosphatase 2A Facilitates DNA Double-Strand Break Repair. *Mol. Cell* **20**, 801-809 (2005).

S7. Castrillon, D.H., Miao, L., Kollipara, R., Horner, J.W., & DePinho, R.A. Suppression of ovarian follicle activation in mice by the transcription factor Foxo3a. *Science* **301**, 215-218 (2003).

S8. Miyamoto, K. *et al.* Foxo3a is essential for maintenance of the hematopoietic stem cell pool. *Cell Stem Cell* **1**, 1-12 (2007).

S9. Matsuoka, S. *et al*. ATM and ATR substrate analysis reveals extensive protein networks responsive to DNA damage. *Science* **316**, 1160-1166 (2007).

S10. Lim, D. S. *et al.* ATM phosphorylates p95/nbs1 in an S-phase checkpoint pathway. *Nature* **404**, 613-617 (2000).

S11. Wu, X. *et al*. ATM phosphorylation of Nijmegen breakage syndrome protein is required in a DNA damage response. *Nature* **405**, 477-482 (2000).

S12. Zhao, S. *et al.* Functional link between ataxia-telangiectasia and Nijmegen breakage syndrome gene products. *Nature* **405**, 473-477 (2000).

S13. Difilippantonio, S. *et al*. Distinct domains in Nbs1 regulate irradiation-induced checkpoints and apoptosis. *J. Exp. Med*. **204**, 1003-1011 (2007).

S14. Difilippantonio, S. *et al*. Role of Nbs1 in the activation of the Atm kinase revealed in humanized mouse models. *Nat. Cell Biol*. **7**, 675-685 (2005).

S15. Lee, J. H., & Paull, T. T. Direct activation of the ATM protein kinase by the Mre11/Rad50/Nbs1 complex. *Science* **304**, 93-96 (2004).

S16. Uziel, T. *et al*. Requirement of the MRN complex for ATM activation by DNA damage. *EMBO J*. **22**, 5612-5621 (2003).

S17. Contessa, J. N. *et al.* Ionizing radiation activates Erb-B receptor dependent Akt and p70 S6 kinase signaling in carcinoma cells. *Oncogene* **21**, 4032-4041 (2002).

S18. Kao, G. D., Jiang, Z., Fernandes, A. M., Gupta, A. K., & Maity A. Inhibition of phosphatidylinositol-3-OH kinase/Akt signaling impairs DNA repair in glioblastoma cells following ionizing radiation. *J. Biol. Chem*. **282**, 21206-21212 (2007).

S19. Khanna, K.K. *et al.* ATM associates with and phosphorylates p53: mapping the region of interaction. *Nat. Genet*. **20**, 398-400 (1998).

S20. Salvador, J.M. *et al*. Mice lacking the p53-effector gene Gadd45a develop a lupus-like syndrome. *Immunity* **16**, 499-508 (2002).

S21. Takai, H. *et al*. Chk2-deficient mice exhibit radioresistance and defective p53-mediated transcription. *EMBO J*. **21**, 5195–5205 (2002).

S22. Ziegler, K. *et al*. A rapid in vitro polyomavirus DNA replication assay. *J*. *Virol*. *Methods* **122**, 123-127 (2004).